Virial expansions for quantum plasmas: Maxwell-Boltzmann statistics

Angel Alastuey,[1] Françoise Cornu,[2] and Asher Perez[1]
[1]*Laboratoire de Physique, Unité de Recherche Associée No. 1325 au Centre National de la Recherche Scientifique, Ecole Normale Supérieure de Lyon, 46 allée d'Italie, 69364 Lyon Cedex 07, France*
[2]*Laboratoire de Physique Théorique–ENSLAPP, Unité de Recherche Associée No. 1436 au Centre National de la Recherche Scientifique, Ecole Normale Supérieure de Lyon, 46 allée d'Italie, 69364 Lyon Cedex 07, France*
(Received 16 March 1994)

This paper is devoted to the calculation of the density expansions (at fixed temperature) of the Maxwell-Boltzmann thermodynamic functions for a quantum plasma. We start from a standard identity that relates the free energy to the particle correlations. These correlations are represented by diagrammatic series, which have been introduced in a previous paper. In the corresponding graphs, the ordinary points are replaced by extended objects, the filaments, which are linked by resummed bonds depending on the particle densities ρ. A scaling analysis of the spatial integrals involved in the graphs shows that the free energy can be represented by a double integer series in $\rho^{1/2}$ and $\ln\rho$. Furthermore, we derive simple rules that give the leading order in ρ of the contribution from every previous graph. The exact density expansion of the free energy is explicitly calculated up to order $\rho^{5/2}$. In the corresponding expression, the contributions of various physical effects, such as screening, diffraction, or recombination, are clearly identified. At the order ρ^2, we recover the expansion obtained via the effective-potential method. Our present terms of order $\rho^{5/2}$ correctly reproduce results that are known in some particular limits.

PACS number(s): 05.30.−d, 05.70.Ce, 52.25.Kn

I. INTRODUCTION

This paper is the second of a series devoted to the study of the density expansions of the thermodynamic quantities for quantum plasmas. We consider a multicomponent system $\mathcal{S}$ made of electrons and nuclei that are assumed to be point particles. Each particle has a mass m_α and carries a charge e_α and a spin σ_α where α is a species index that specifies the nature of the particle. The Hamiltonian of $\mathcal{S}$ is nonrelativistic and only involves two-body Coulomb interactions of the form $e_\alpha e_\beta / r$ for two charges separated by a distance r. It does not depend on the spins of the particles. Such a purely Coulombic description of matter is well suited for a very large variety of physical situations. Beside their own conceptual interest, the virial expansions are useful in practice for studying regimes where the density is not too high and the temperature is not too low (for instance these conditions are met in the core of the sun).

In an earlier paper [1] (hereafter referred to as paper I), we derived a diagrammatic representation for the particle correlations of $\mathcal{S}$ in the framework of Maxwell-Boltzmann statistics. As in the work by Ginibre [2], the application of the Feynman-Kac formula [3] to the density matrix leads to the introduction of an auxiliary classical system $\mathcal{S}^*$ made of closed filaments. Since the filaments interact via two-body forces, all the familiar diagrammatical methods [4] can be applied to $\mathcal{S}^*$. However, the corresponding Mayer-like graphs diverge because of the long-range Coulombic nature of the interaction potential between two filaments. These long-range divergencies are removed via the chain resummations first introduced by Mayer [5] and Salpeter [6] for classical point charges. In fact, inspired by the works of Meeron [7] and Abe [8] for classical Coulomb systems, we have shown that the whole set of Mayer graphs defining the correlations of $\mathcal{S}^*$ can be transformed exactly into a new set of prototype graphs Π built with resummed bonds. This provides a well-behaved diagrammatic representation for the particle correlations of $\mathcal{S}$, where the integrability of each graph is guaranteed by a sufficiently fast decay of the resummed bonds. We stress that some resummed bonds decay only algebraically in agreement with the absence of exponential screening in the quantum case [9,10].

In the present paper, the above diagrammatical representation is used for studying the density expansions of the Maxwell-Boltzmann thermodynamic functions (at fixed inverse temperature β) in a systematic way. On the basis of simple scaling arguments, we show that the virial expansions involve half-integer powers of the densities and integer powers of the logarithm of the densities. (The presence of logarithmic terms was first conjectured by Friedman [11].) We also give detailed prescriptions for selecting the graphs (in finite number) that contribute to a given order in ρ where ρ is a generic notation for the particle densities. This allows us to recover the known results up to order ρ^2, and to calculate exactly the next term of order $\rho^{5/2}$.

As announced previously [1], the above expansions are term-to-term well defined despite the macroscopic collapse of the Maxwell-Boltzmann (MB) system [12]. In a future paper, the exchange contributions due to Fermi or Bose statistics will be evaluated via a perturbative

 ©1995 The American Physical Society

scheme, in which the MB quantities are the reference ingredients. A brief description of this scheme has been already given [13], as well as the complete form of the virial expansion up to order $\rho^{5/2}$.

The present paper is organized as follows. In Sec. II, we recall the form of the diagrammatic representation for the particle correlations. The topological rules, statistical weights, and resummed bonds defining the Π graphs are explicited.

In Sec. III, we study the general structure of the density expansion of the free energy. We start from a standard identity, which expresses the free energy in terms of the particle correlations via an integral over a coupling parameter. Inserting the above Π representation into this identity, we rewrite the free energy as a sum of Π contributions. Simple arguments suggest that the contribution of each graph can be expanded in a double integer series in $\rho^{1/2}$ and $\ln\rho$. This nonanalytic structure reflects the screening of the bare Coulomb potential. The half powers of ρ are linked to partial scaling of the resummed bonds with respect to the Debye length $\kappa^{-1}=(4\pi\beta\sum_\alpha e_\alpha^2\rho_\alpha)^{-1/2}$. The logarithms arise from the presence of $1/r^3$ tails in some bonds. We give simple rules for evaluating the order in the density of the leading contribution of any graph. Roughly speaking, the latter increases with the number of points and the number of resummed bonds. Only a finite number of graphs then contributes to a given term in the density expansion of the free energy.

The explicit calculations are carried out up to order $\rho^{5/2}$ in Sec. IV. The contributions of the various physical effects mentioned in paper I, can be clearly identified. There are purely classical terms that arise from Debye screening at large distances. The short-range quantum effects associated to bound and scattering states enter in suitably truncated traces of the quantum Gibbs factors for a finite number of charges. Eventually, there are diffraction terms that appear as quantum corrections to a classical treatment of the long-range part of the interactions. All these physical effects should be coupled together at higher orders in the density. Comparisons to previous results and checkings are briefly described.

The other thermodynamic functions are considered in Sec. V. Their density expansions can be obtained from that of the free energy via partial differentiations with respect to the temperature or the densities. In particular, we calculate the pressure up to order $\rho^{5/2}$.

Of course, the virial expansions can be also studied by using other first-principles formalisms. First, the effective-potential method formulated by Morita [14] for quantum systems with two-body interactions, has been applied to the present Coulomb case by Ebeling [15]. This method consists in introducing classical equivalent systems made of point objects with two-, three-, and higher-order many-body effective interactions. In practice, only two-body effective potentials have been retained [15–17]. This amounts to considering well-behaved classical systems with two-body Coulomb interactions that are regularized at short distances. (Quantum effects smooth out the singularity of $1/r$ at the origin.) The corresponding calculations [16,17] provide the exact form of the virial expansions up to order ρ^2, which is indeed recovered by our formalism [13]. However, the expressions proposed for the $\rho^{5/2}$ term [17] are not complete because the three-body effective potentials do contribute at this order [18]. Our formalism allows a precise evaluation of this missing contribution, which is of the diffraction type. We stress that the presence of this additional diffraction term is crucial for recovering the Wigner-Kirkwood $\hbar^2$ corrections [19] to the classical quantities for the one-component plasma. By the way, we also do recover the virial expansion for the classical one-component plasma calculated by Cohen and Murphy [20].

Another possible approach is based on the standard many-body perturbative expansions with respect to the Coulomb interaction potential $v_c(r)=1/r$ in the framework of the grand-canonical ensemble. These expansions can be written in terms of graphs similar to those that appear in field theory, where fermionic or bosonic loops associated to imaginary-time free propagators are connected at different times by an arbitrary number of interaction lines v_c [21]. The long-range Coulomb divergencies are eliminated via the well-known ring resummations [22,23]. To our knowledge, analytic evaluations of the corresponding Feynman graphs have been restricted to the high-density regime at zero temperature [22], and to the high-temperature limit [24]. Explicit calculations of the virial coefficients at finite nonzero temperature should be also possible by following Rogers's idea [25]. This author proposed a classical treatment of the ring resummations combined with a proper account of the Ladder graphs that describe quantum effects at short distances. In this procedure, some terms are left over since they are expected to be quantitatively small in the physical regimes considered by the author [26] (i.e., at moderately high densities where complex entities made of several charges may be formed). At the moment, we have checked that the high-temperature expansions up to order $\beta^{5/2}$ of our virial coefficients do coincide with the terms found by DeWitt [24].

II. THE PARTICLE CORRELATIONS

In paper I, we have shown that the two-particle correlations $\rho_T(\alpha_a\mathbf{r}_a,\alpha_b\mathbf{r}_b)$ of $\mathcal{S}$ can be represented by the diagrammatic series

$$\rho_T(\alpha_a\mathbf{r}_a,\alpha_b\mathbf{r}_b)=\sum_\Pi \frac{1}{S_\Pi}\int \mathcal{D}(\xi_a)\mathcal{D}(\xi_b)\rho(\mathcal{E}_a)\rho(\mathcal{E}_b) \times\int\prod_{n=1}^{N} d\mathcal{P}_n\rho(\mathcal{P}_n)\left[\prod F\right]_\Pi , \tag{2.1}$$

where the ordinary points are replaced by filaments. Each graph Π is made of the two root filaments $\mathcal{E}_a$ and $\mathcal{E}_b$, and of N internal filaments $\mathcal{P}_n$ ($N=0,\ldots,\infty$). The state of each filament is characterized by its species index α, its position $\mathbf{r}$, and its shape. The latter is parametrized

by $\lambda_\alpha\xi(s)$ $(0\le s\le 1)$ where $\lambda_\alpha=(\beta\hbar^2/m_\alpha)^{1/2}$ is the de Broglie wavelength of species α and $\xi(s)$ is a Brownian bridge subjected to the constraint $\xi(0)=\xi(1)=\mathbf{0}$. The phase-space measure $d\mathcal{P}$ means a discrete summation over α combined to a spatial integration over $\mathbf{r}$, and a functional integration over $\xi(s)$ with the normalized Gaussian measure $\mathcal{D}(\xi)$ defined by its covariance

$$\int\mathcal{D}(\xi)\xi_\mu(s)\xi_\nu(t)=\delta_{\mu\nu}\times\begin{cases}s(1-t), & s\le t\\ t(1-s), & t\le s\end{cases}. \tag{2.2}$$

(ξ_μ is the component of ξ along the μ axis.)

The topological prescriptions that define the graphs Π are similar to that of the familiar Mayer graphs. Each graph Π is connected and contains no articulation filament. Two filaments are linked by at most one resummed F bond. $[\prod F]_\Pi$ is the product of the F bonds in the graph Π and S_Π is its symmetry factor, i.e., the number of permutations of the internal filaments $\mathcal{P}_n$, which do not change this product. The sum (2.1) runs over all the unlabeled topologically different diagrams Π.

There are four kinds of resummed bonds F. Two of them are short ranged and proportional to the screened charge-charge and screened dipole-charge potential between the filaments $\mathcal{P}_i$ and $\mathcal{P}_j$, i.e.,

$$F_{cc}(\mathcal{P}_i,\mathcal{P}_j)=f_D=-\beta e_{\alpha_i}e_{\alpha_j}\phi_D(|\mathbf{r}_i-\mathbf{r}_j|) \tag{2.3}$$

and

$$F_{dc}(\mathcal{P}_i,\mathcal{P}_j)=\lambda_{\alpha_i}\xi_i\cdot\nabla_i f_D =-\beta e_{\alpha_i}e_{\alpha_j}\int_0^1 ds\,\lambda_{\alpha_i}\xi_i(s)\cdot\nabla_i\phi_D(|\mathbf{r}_i-\mathbf{r}_j|)\,. \tag{2.4}$$

In (2.3) and (2.4), ϕ_D is the usual Debye potential

$$\phi_D(r)=\frac{\exp(-\kappa r)}{r}\,. \tag{2.5}$$

The other two resummed bonds reduce to

$$f_{\rm dip}(\mathcal{P}_i,\mathcal{P}_j)=-\beta e_{\alpha_i}e_{\alpha_j}\int_0^1 ds\int_0^1 ds'(\lambda_{\alpha_i}\xi_i(s)\cdot\nabla_i)\times(\lambda_{\alpha_j}\xi_j(s')\cdot\nabla_j)\times(\phi_D-v_c)(r_{ij}) \tag{2.6}$$

and

$$f_R(\mathcal{P}_i,\mathcal{P}_j)=\exp\left\{-\beta e_{\alpha_i}e_{\alpha_j}(\phi_D-v_c)(r_{ij})-\beta e_{\alpha_i}e_{\alpha_j}\int_0^1 ds[v_c(|\mathbf{r}_i+\lambda_{\alpha_i}\xi_i(s)-\mathbf{r}_j-\lambda_{\alpha_j}\xi_j(s)|)\right.$$
$$+(\lambda_{\alpha_i}\xi_i(s)\cdot\nabla_i+\lambda_{\alpha_j}\xi_j(s)\cdot\nabla_j)(\phi_D-v_c)(r_{ij})]$$
$$\left.-\beta e_{\alpha_i}e_{\alpha_j}\int_0^1 ds\int_0^1 ds'(\lambda_{\alpha_i}\xi_i(s)\cdot\nabla_i)(\lambda_{\alpha_j}\xi_j(s')\cdot\nabla_j)(\phi_D-v_c)(r_{ij})\right\}$$
$$-1+\beta e_{\alpha_i}e_{\alpha_j}\phi_D(r_{ij})+\beta e_{\alpha_i}e_{\alpha_j}\int_0^1 ds(\lambda_{\alpha_i}\xi_i(s)\cdot\nabla_i+\lambda_{\alpha_j}\xi_j(s)\cdot\nabla_j)\phi_D(r_{ij})$$
$$+\beta e_{\alpha_i}e_{\alpha_j}\int_0^1 ds\int_0^1 ds'(\lambda_{\alpha_i}\xi_i(s)\cdot\nabla_i)(\lambda_{\alpha_j}\xi_j(s')\cdot\nabla_j)(\phi_D-v_c)(r_{ij})\,, \tag{2.7}$$

and decay only as $1/r_{ij}^3$ when $r_{ij}\to\infty$. Each of the resummed bonds may link any pair of filaments with the sole restriction that the convolution structures $F_{cc}\circ F_{cc}$, $F_{dc}\circ F_{cc}$, $F_{cc}\circ F_{cd}$, and $F_{dc}\circ F_{cd}$ are excluded (this avoids double counting).

The statistical weights of the filaments in the graphs Π are the filament densities $\rho(\mathcal{E})$, which are complicated functionals of the shapes of the filaments, i.e., $\rho(\mathcal{E})=\rho_\alpha(\xi)$. These functionals are determined from their expansions with respect to the particle densities, which reduce to double integer series in $\rho^{1/2}$ and $\ln\rho$. The first two terms of these series read

$$\rho_\alpha(\xi)=\rho_\alpha+\sum_\beta\rho_\alpha\rho_\beta\int d\mathbf{r}\int\mathcal{D}(\xi_1)\left\{\exp\left[-\beta e_\alpha e_\beta\int_0^1 ds\,v_c(|\mathbf{r}+\lambda_\beta\xi_1(s)-\lambda_\alpha\xi(s)|)\right]\right.$$
$$\left.-\int\mathcal{D}(\xi')\exp\left[-\beta e_\alpha e_\beta\int_0^1 ds\,v_c(|\mathbf{r}+\lambda_\beta\xi_1(s)-\lambda_\alpha\xi'(s)|)\right]\right\}+O(\rho^{5/2})\,. \tag{2.8}$$

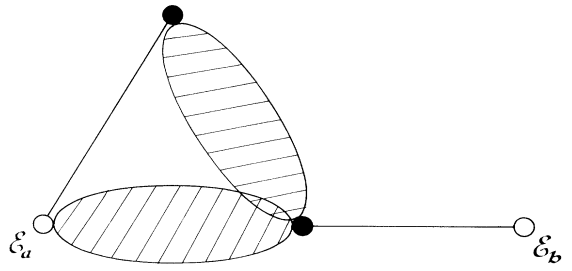

FIG. 1. A typical graph Π, which contributes to $\rho_T(\mathcal{C}_a,\mathcal{C}_b)$. The white circles represent the root filaments $\mathcal{C}_a$ and $\mathcal{C}_b$, while the black circles denote field filaments. The solid lines and the hatched bubbles are, respectively, Debye and f_R bonds.

In Fig. 1, we draw a typical graph Π, which contributes to (2.1) (for clarity, the filaments are merely represented by circles).

The diagrammatic representation (2.1) is the quantum extension of the expansion first derived by Meeron [7] for classical systems. Indeed, in the classical limit $\hbar\to 0$, the bonds F_{cd} and $f_{\rm dip}$ vanish, while f_R and $\rho_\alpha(\xi)$ reduce to $[\exp(f_D)-1-f_D]$ and ρ_α, respectively. The graphs Π then become identical to the classical Meeron graphs.

III. THE FREE ENERGY

A. Principle of the method

The free energy $(\beta F/\Lambda)$ per unit of volume and in units of $k_B T$, is related to the particle correlations via

$$\frac{\beta F}{\Lambda}-\frac{\beta F_{\rm id}}{\Lambda}=\frac{1}{2}\sum_{\alpha_a,\alpha_b}\beta e_{\alpha_a}e_{\alpha_b}\int_0^1 dg\int d\mathbf{r}\,\rho_{T,g}(\alpha_a\mathbf{0},\alpha_b\mathbf{r})\frac{1}{r}\ . \tag{3.1}$$

In this identity, g is a dimensionless coupling parameter, while $\rho_{T,g}(\alpha_a\mathbf{0},\alpha_b\mathbf{r})$ is the two-point correlation of the system $\mathcal{S}_g$ where the coupling between two charges e_α and e_β is multiplied by g and becomes $ge_\alpha e_\beta$ ($F_{\rm id}$ is the free energy of the ideal system $\mathcal{S}_{g=0}$). Furthermore, the temperature and the particle densities of the systems $\mathcal{S}_g$ are identical to those of the genuine system $\mathcal{S}$ corresponding to $g=1$.

The required density expansion of the free energy will be calculated by inserting the Π representation (2.1) of $\rho_{T,g}$ in the right-hand side of (3.1). The corresponding contribution of a given prototype diagram Π reads (with obvious notations)

$$\tfrac{1}{2}\beta e_\alpha e_{\alpha_\beta}\int_0^1 dg\int d\mathbf{r}\frac{1}{r}\Pi_g(r)\ , \tag{3.2}$$

with

$$\Pi_g(r)=\int\mathcal{D}(\xi_a)\mathcal{D}(\xi_b)\rho_g(\mathcal{C}_a)\rho_g(\mathcal{C}_b)\Pi_g(\mathbf{r},\xi_a,\xi_b)\ . \tag{3.3}$$

The subscript g means that the resummed bonds in Π are calculated with the coupling constant ge_ie_j instead of e_ie_j (consequently, κ is changed into $\sqrt{g}\,\kappa$) like the statistical weights $\rho_g(\mathcal{C})$. Each contribution (3.2) can be itself expanded in powers of the particle densities because of the following two mechanisms. First, as noticed in Sec. II, the functionals $\rho_g(\mathcal{C})$ have to be replaced by double integer series in $\rho^{1/2}$ and $\ln\rho$. Second, the distance dependence of some resummed bonds is scaled by the Debye length $(\sqrt{g}\,\kappa)^{-1}=(4\pi g\beta\sum_\alpha e_\alpha^2\rho_\alpha)^{-1/2}$. Thus, as shown in the Sec. III B, the space integrations in Π provide series in κ, whose structure is independent of the precise form of the functional $\rho_g(\mathcal{C})$. This allows us to determine the general form of the contribution (3.2).

B. General structure of the density expansion

First, we study the density dependence of the spatial integrations over the positions of the field filaments in (3.2), which is related to the scaling properties of the resummed bonds with respect to κ^{-1}. This analysis does not depend neither on the coupling parameter g nor on the internal degrees of freedom $(\alpha,\xi(s))$ of the filaments. So, in the meantime, we omit part of the dependences with respect to g, the shapes $\xi(s)$ of the filaments, and their species nature α, which are considered as given parameters. These dependences will be easily reestablished at the end of Sec. III B, where we will show that the integration over g, the summations over α, and the functional integrations over $\xi(s)$, with the measure $\mathcal{D}(\xi)\rho_b(\mathcal{C})$, do not modify the structure of the density expansion of the spatial contribution to (3.2).

In fact, the present analysis is strictly identical to that of the resummed graphs in the fugacity expansion of $\rho(\mathcal{C})$ [1]. So, here, we just describe the basic outlines of the method. In particular, we give the scaling decompositions of the resummed bonds F, which are quite useful in the following. The bonds (2.3), (2.4), and (2.6) are obviously scaled by κ^{-1}, i.e.,

$$f_D=-\kappa\beta_{ij}\frac{e^{-x}}{x}\ , \tag{3.4}$$

$$\lambda_{\alpha_i}\xi_i\cdot\nabla_i f_D=\kappa^2\beta_{ij}\lambda_{\alpha_i}\int_0^1 ds(\xi_i(s)\cdot\hat{\mathbf{x}})\left[\frac{e^{-x}}{x}+\frac{e^{-x}}{x^2}\right]\ , \tag{3.5}$$

$$f_{\rm dip}=\kappa^3\beta_{ij}\lambda_{\alpha_i}\lambda_{\alpha_j}\int_0^1 ds\int_0^1 ds'\left[(\xi_i(s)\cdot\xi_j(s'))\left[\frac{1-e^{-x}-xe^{-x}}{x^3}\right]-(\xi_i(s)\cdot\hat{\mathbf{x}})(\xi_j(s')\cdot\hat{\mathbf{x}})\frac{(3-3e^{-x}-3xe^{-x}-x^2e^{-x})}{x^3}\right]\ , \tag{3.6}$$

with $\mathbf{x}=\kappa(\mathbf{r}_i-\mathbf{r}_j)$ and $\beta_{ij}=\beta e_i e_j$. However, the bond f_R is not entirely scaled by κ^{-1} since it is not proportional to a dimensionless integrable function of $\mathbf{x}$ only. (Otherwise, the present analysis would be immediately performed by making the variable changes $\mathbf{r}_i \to \mathbf{x}_i=\kappa\mathbf{r}_i$ in II.) In fact, the spatial behavior of f_R is also controlled by the Landau lengths $l_{\alpha\beta}=\beta e_\alpha e_\beta$ and the de Broglie wavelengths λ_α. These lengths only depend on the temperature and remain fixed in the zero-density limit. In order to disentangle the various scales associated to κ^{-1}, $\beta e_\alpha e_\beta$, and λ_α, it is convenient to rewrite f_R as $(\mathbf{r}=\mathbf{r}_i-\mathbf{r}_j)$

$$f_R=f_T(\xi_i,\xi_j;\mathbf{r})+f_T(\xi_i,\xi_j;\mathbf{r})\sum_{n=1}^{\infty}\kappa^n H_n(\xi_i,\xi_j;\mathbf{x}) + \sum_{n=2}^{\infty}\kappa^n G_n(\xi_i,\xi_j;\mathbf{x}) , \tag{3.7}$$

with

$$f_T(\xi_i,\xi_j;\mathbf{r})=\exp\left[-\beta_{ij}\int_0^1 ds\, v_c(|\mathbf{r}+\lambda_i\xi_i(s)-\lambda_j\xi_j(s)|)\right] -1+\frac{\beta_{ij}}{r}-\frac{\beta_{ij}^2}{2r^2} +\beta_{ij}\int_0^1 ds(\lambda_{\alpha_i}\xi_i(s)\cdot\nabla-\lambda_{\alpha_j}\xi_j(s)\cdot\nabla)\frac{1}{r} , \tag{3.8}$$

while the κ-scaled functions H_n and G_n can be calculated from (2.7). For instance, we find

$$H_1(\xi_i,\xi_j;\mathbf{x})=H_1(x)=-\beta_{ij}\frac{(e^{-x}-1)}{x} , \tag{3.9}$$

$$G_2(\xi_i,\xi_j;\mathbf{x})=G_2(x)=\frac{\beta_{ij}^2}{2}\frac{e^{-2x}}{x^2} , \tag{3.10}$$

$$G_3(\xi_i,\xi_j;\mathbf{x})=\frac{\beta_{ij}^3}{6}\frac{(1-e^{-3x})}{x^3} +\beta_{ij}^2\int_0^1 ds(\lambda_{\alpha_i}\xi_i(s)\cdot\hat{\mathbf{x}}-\lambda_{\alpha_j}\xi_j(s)\cdot\hat{\mathbf{x}}) \times\left[\frac{1-(1+x)e^{-2x}}{x^3}\right] . \tag{3.11}$$

The functions G_n are integrable at large distances as the functions H_n for $n\geq 4$ since they decay at most as $1/x^n$ for x large. The truncated bond f_T does not depend on κ^{-1}, and is scaled by the above temperature-dependent lengths.

The decompositions (3.4)–(3.7) with respect to the various scales are quite useful for our purpose, because they provide a series representation of any graph II in terms of graphs where all bonds are scaled either by κ^{-1} or by the fixed lengths $\beta e_\alpha e_\beta$ and λ_α. These graphs are called scaling-decomposed graphs and noted G_Π^{scaled}. Each prototype diagram II with one or more bonds f_R generates an infinite set of graphs G_Π^{scaled}. If II is made with only κ-scaled bonds, there is only one graph G_Π^{scaled}, identical to II of course. In Fig. 2, we show four graphs G_Π^{scaled} arising in the scaling decomposition of the diagram II drawn in Fig. 1.

In each graph G_Π^{scaled}, the long-range Coulomb divergencies are removed because all the terms in the decompositions (3.4)–(3.7) decay at least as $1/r^3$ at large distances. However, there may appear spurious nonintegrable singularities at short distances because some of these terms diverge at the origin. These unphysical divergencies, also present in the classical Abe-Meeron graphs [27], are eliminated by suitably collecting together the dangerous contributions (see Sec. IV C for an example). The corresponding procedure is a pure mathematical artifact and does not reflect any density-dependent many-body effect. Consequently, the structure of the κ expansion of the spatial integrals in each G_Π^{scaled} can be determined without any explicit consideration of the previous short-range divergencies. The analysis is carried out in Fourier space with the help of the generalized Plancherel identity. The spatial contribution of each G_Π^{scaled}, and consequently of any graph II, reduces to a double integer series in κ and $\ln\kappa$. Only integer powers of κ appear because both large-r expansion of f_T and small-r expansions of G_n and H_n involve only integer powers of r. Moreover, the logarithms arise in part from the $1/r^3$ tail in f_T.

Now, we turn to the functional integrations over the shapes of the filaments of the spatial contribution to (3.2). As argued in paper I, the general term in the density ex-

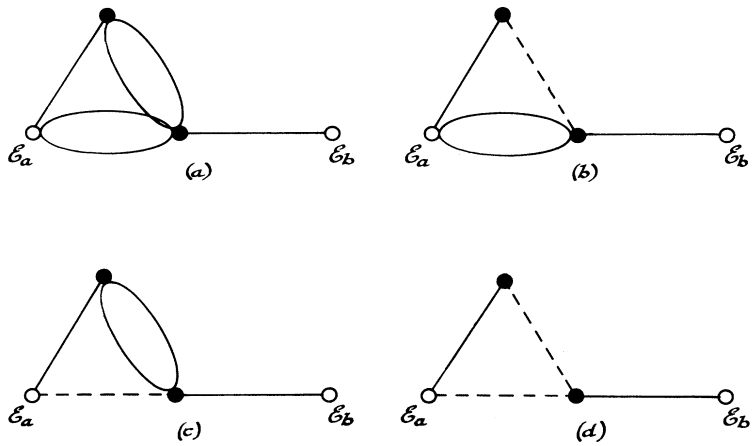

FIG. 2. Four graphs G_Π^{scaled}, which arise in the scaling decomposition of the graph II shown in Fig. 1. The double solid lines (bubbles) represent bonds $f_D^2/2$ while the dashed lines are bonds f_T.

pansion of the functional $\rho_g(\mathscr{E})$ around ρ_α is a product of integer powers of ρ, κ, and $\ln\kappa$, by functionals of ξ, which only depend on the temperature (and on the coupling parameter g of course). The structure of the density expansion of the previous spatial contribution is identical, because the ξ dependence of the functions H_n and G_n only enters as polynomials in ξ, which multiply functions of x. (The ξ dependence of the function f_T is more complicated but does not play any role since f_T does not depend on the density.) Therefore, the functional integrations over the ξ_i's weighted by $\rho_g(\mathscr{E}_i)$ may be factored in each term of order $\rho^l\kappa^n\ln^p\kappa$ (with l,n,p integers) and does not change the structure of the density expansion [some terms may disappear because of the parity of the measure $\mathscr{D}(\xi)\rho_g(\mathscr{E})$]. Since κ_g is proportional to $g^{1/2}$, the integration over the coupling parameter g in (3.2) is also factored out in each term of order $\rho^l\kappa^n\ln^p\kappa$, while the discrete summations over the species may only kill some terms because of the neutrality condition $\sum_\alpha e_\alpha\rho_\alpha=0$. The density expansion of the excess free energy (3.1) finally reads

$$\frac{\beta F}{\Lambda}-\frac{\beta F_{\rm id}}{\Lambda}=\sum_{l,n,p}P_l\{\rho_\alpha\}\left[4\pi\beta\sum_\alpha e_\alpha^2\rho_\alpha\right]^{n/2}\times\ln^p\left[\text{const}\times 4\pi\beta\sum_\alpha e_\alpha^2\rho_\alpha\right], \tag{3.12}$$

where $P_l\{\rho_\alpha\}$ are homogeneous polynomials of degree l in the densities ρ_α with coefficients depending on the temperature, while the "constants" in the arguments of the logarithmic terms are built with the temperature-dependent lengths $\beta e_\alpha e_\beta$ and λ_α.

C. Leading Π contribution

Now we turn to the evaluation of the leading contribution of a given prototype graph Π. In fact, we just sketch the main arguments that allow such an evaluation in the most general case. The precise order of this leading contribution is estimated only in a few simple cases. Like in Sec. III B, the central part of the analysis relies in the determination of the density dependence of the spatial integrals over the filament positions involved in (3.2). Consequently, in the meantime, the dependences with respect to the filament shapes, the species indexes, and the coupling parameter g are not explicitly taken into account. In particular, the filaments are assimilated to points. The effects of the integrations and summations over the omitted variables will be briefly mentioned at the end of the method. All the eventual logarithmic terms are considered to be of order $\rho^0=1$.

For the present analysis, it is convenient to introduce the following numbers: N (internal points), M_R (bonds f_R), M_D (bonds f_D), M_D' (bonds $\lambda_{\alpha_i}\xi_i\cdot\nabla_i f_D$), M_D'' (bonds $f_{\rm dip}$), and $M=M_R+M_D+M_D'+M_D''$ (F bonds). Since each $\rho_g(\mathscr{E}_i)$ is at least of order ρ, according to the expansion (2.8), the product of the statistical weights in a graph Π is at least of order ρ^{N+2}. The scaling decomposition (3.7) shows that the lowest order contributions arise from $\kappa^2G_2(x)=f_D^2/2$ and f_T because f_T is integrable [except for possible logarithmic singularities, which ultimately give $\ln(\text{const}\times\kappa)$ terms]. Indeed, all the other κ-scaled terms in (3.7) are at least of order κ^3, while the mixed functions $\kappa^nH_nf_T$ with $n\geq 1$ introduce κ^n multiplicative factor to the bare contribution of f_T. Therefore, the lowest-order contribution to (3.2) is given by one of the decomposed graphs $G^{\rm scaled}_{\Pi,\min}$ with M_T bonds f_T and (M_R-M_T) bonds $\kappa^2G_2(x)$. For instance, in the case of the graph Π ($N=2,M_R=2,M_D=2,M_D'=0,M_D''=0$) shown in Fig. 1, the lowest-order $G^{\rm scaled}_{\Pi,\min}$ graphs are those drawn in Fig. 2.

Since f_T is integrable and entirely controlled by the lengths $\beta e_\alpha e_\beta$ and λ_α, which do not depend on the density, the dominant space configurations in $G^{\rm scaled}_{\Pi,\min}$ are such that each pair $\{ij\}$ connected by a f_T bond is contained in a "contraction" disk with a finite radius σ, which only depends on the temperature. In the low-density limit, κ^{-1} is large compared to σ and the κ-scaled bonds f_D, $f_D^2/2$, $\lambda_{\alpha_i}\xi_i\cdot\nabla_i f_D$, and $f_{\rm dip}$, which connect part of the points belonging to the same contraction disk, can be replaced by their respective short-distance forms $-\beta_{ij}/r$, $-\beta_{ij}^2/(2r^2)$, $-\beta_{ij}\lambda_{\alpha_i}\xi_i\cdot\nabla_i(1/r_{ij})$, and $-\beta_{ij}\kappa^2(\lambda_{\alpha_i}\xi_i\cdot\nabla_i)(\lambda_{\alpha_j}\xi_j\cdot\nabla_j)r_{ij}/2$. Therefore, the order of the contribution of $G^{\rm scaled}_{\Pi,\min}$ is directly related to the one of the contracted graph made with disks of radius σ located at $\mathbf{R}_i$ and connected by the remaining κ-scaled bonds. For the graphs $G^{\rm scaled}_{\Pi,\min}$ shown in Fig. 2, this first step of the contraction process leads to the graphs represented in Fig. 3. (The points that do not enter in the contraction

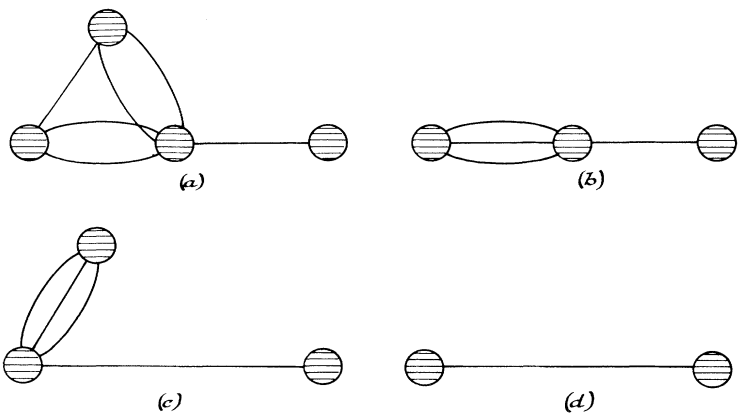

FIG. 3. The four contracted graphs, which are obtained from the graphs shown in Fig. 2 after the first step of the contraction process. The big hatched circles are contraction disks. Each solid line represents a bond f_D.

procedure can be also replaced by disks.)

At this level, in a contracted graph derived from a $G^{\text{scaled}}_{\Pi,\min}$, some disks may be connected by products of κ-scaled bonds involving at least either three f_D bonds; two f_D bonds and one f_{dip} bond; one f_D bond and two f_{dip} bonds; one f_D bond and one $\lambda\xi\cdot\nabla f_D$ bond; three f_{dip} bonds; two f_{dip} bonds and one $\lambda\xi\cdot\nabla f_D$ bond; one f_{dip} bond and one $\lambda\xi\cdot\nabla f_D$ bond; or two $\lambda\xi\cdot\nabla f_D$ bonds. All these products decay at least as $1/r^3$ over a length scale $\sigma \ll \kappa^{-1}$, which does not depend on the density, so the corresponding disks can be themselves contracted into a single one. We point out that f_{dip} behaves as κ^2/r for $r\sim\sigma$, while f_{dip} decays as $1/r^3$ for r large compared to κ^{-1}. For instance, Figs. 3(b) and 3(c) are transformed into Fig. 3(d), while 3(a) and 3(d) remain unchanged in the second step of the contraction. At the end of this contraction process, the contracted disks that are left over are connected either by a single f_D bond, two f_D bonds, one f_D bond and one f_{dip} bond, a single f_{dip} bond, two f_{dip} bonds, or a single $\lambda\xi\cdot\nabla f_D$ bond.

If $M_T < N+1$, the contracted graph resulting from $G^{\text{scaled}}_{\Pi,\min}$ contains N_d disks with $N_d \le N+2-M_T$, $M_D^{\text{cont}} f_D$ bonds with $0 \le M_D^{\text{cont}} \le M_D + 2(M_R - M_T)$, $M_D'^{\text{cont}}\lambda\xi\cdot\nabla f_D$ bonds with $0 \le M_D'^{\text{cont}} \le M_D'$, and $M_D''^{\text{cont}} f_{\text{dip}}$ bonds with $0 \le M_D''^{\text{cont}} \le M_D''$. In the contraction procedure, the order of the contribution of $G^{\text{scaled}}_{\Pi,\min}$ remains unchanged when f_D bonds and $\lambda\xi\cdot\nabla f_D$ bonds are absorbed because their respective short-range behaviors at distances $r\sim\sigma$ do not depend on the density. On the contrary, each absorption of one f_{dip} bond introduces a multiplicative factor κ^2. Therefore, the order of the contribution of $G^{\text{scaled}}_{\Pi,\min}$ is equal to the one of the contracted graph multiplied by $\rho^{(M_D''-M_D''^{\text{cont}})}$. The order of the remaining integrals over the (N_d-1) positions $\mathbf{R}_i$ of the contraction disks, which are integrated over in (3.2), is easily determined via the variable change $\mathbf{X}_i=\kappa\mathbf{R}_i$. In this simple scaling transformation, each integration volume $d\mathbf{R}_i$ gives a factor κ^{-3}, while, according to (3.4)–(3.6), each of the bonds f_D, $\lambda\xi\cdot\nabla f_D$, and f_{dip} gives factors κ, κ^2, and κ^3, respectively. Moreover, the potential term $1/r$ in (3.2) gives a factor $\kappa^{\varepsilon^{\text{cont}}}$ with $\varepsilon^{\text{cont}}=1$ if a and b are not contracted into the same disk and $\varepsilon^{\text{cont}}=0$, otherwise. So, when all the factors arising from the density weights, the absorption of f_{dip} bonds, and the previous scaling transformation are taken into account, the order of the contribution of $G^{\text{scaled}}_{\Pi,\min}$ to (3.2) reduces to ρ^{n_G} with

$$n_G = N+2+M_D''-M_D''^{\text{cont}}-\tfrac{3}{2}(N_d-1) + \tfrac{1}{2}M_D^{\text{cont}}+M_D'^{\text{cont}}+\tfrac{3}{2}M_D''^{\text{cont}}+\tfrac{1}{2}\varepsilon^{\text{cont}} . \quad (3.13)$$

If $M_T > N+1$, the contraction procedure leads to the collapse of all the points of $G^{\text{scaled}}_{\Pi,\min}$ into a single disk. The order of the contribution of $G^{\text{scaled}}_{\Pi,\min}$ to (3.2) reduces then to the one of the weighting prefactor multiplied by $\kappa^{2M_D''}$, i.e., to ρ^{m_G} with

$$m_G = N+2+M_D'' . \quad (3.14)$$

Notice that in the case of short-range forces, the leading order of the Mayer graphs is always ρ^{N+2}.

For similar reasons as those exposed in Sec. III B, the integration over g does not change the above orders, while the functional integrations over the ξ's and the summation over the α's may only kill some contributions. Therefore, strictly speaking, the powers (3.13) and (3.14) should be understood in fact as lower bounds in the present study.

In principle, the order of the leading contribution of any graph Π might be determined by taking either the infimum of the n_G's if $M_R < N+1$, or the infimum of the n_G's and m_G's, otherwise. For instance in the case of the graph Π ($N=2, M_R=2, M_D=2, M_D'=0, M_D''=0$) shown in Fig. 1, the order in ρ of the corresponding four graphs $G^{\text{scaled}}_{\Pi,\min}$ shown in Fig. 2 are, according to (3.13), $n_G^{(a)}=3$ ($N_d=4, M_D^{\text{cont}}=6, \varepsilon^{\text{cont}}=1$) and $n_G^{(b)}=n_G^{(c)}=n_G^{(d)}=\frac{7}{2}$ ($N_d=2, M_D^{\text{cont}}=1, \varepsilon^{\text{cont}}=1$). The leading contribution of this graph Π obviously is of order ρ^3. However, such quantitative evaluations are not easy to carry out, in general, because the determination of the numbers N_d, M_D^{cont}, $M_D'^{\text{cont}}$, $M_D''^{\text{cont}}$, and $\varepsilon^{\text{cont}}$ requires a careful analysis of the topological structure of the considered graph Π. When the graph is highly connected (as it is the case for the bridges), many points may be contracted in the same disk through cascade mechanisms, the control of which is far beyond the scope of the present paper. In the simple case $M_R=0$, there is no contraction, these numbers obviously reduce to $N+2$, M_D, M_D', M_D'', and 1, respectively, and the contribution of Π is exactly of order

$$1+\frac{(M-N)}{2}+\frac{M_D'}{2}+M_D'' . \quad (3.15)$$

It is quite reasonable to assume that the order of the leading contribution of Π is, roughly speaking, an increasing function with respect to the number N of internal points and the number M of F bonds. This assumption is supported by the following simple qualitative arguments. If Π contains a few bonds f_R, the numbers M or/and M_D' and M_D'' are large enough since Π must obey the excluded-convolution rule. In particular, the power (3.15) relative to graphs without any bond f_R do increase with N, because the chain graphs made only with bonds f_D ($M-N=1$, $M_D'=0$, and $M_D''=0$) are not allowed. When Π contains many bonds f_R, the order of the graph $G^{\text{scaled}}_{\Pi,\min}$ with a few functions f_T should be analogous to (3.15) while it reduces to (3.14) if $M_T \ge N+1$: both quantities do exhibit the above monotonicity. Consequently, there is a finite number of graphs that contribute to a given order in the density expansion (3.12) and the minimal power $(l+n/2)$ in (3.12) is $\frac{3}{2}$.

IV. EXPLICIT CALCULATIONS AT THE ORDER $\rho^{5/2}$

According to the general power-counting rules derived in Sec. III C, the graphs Π contributing to the expansion (3.12) up to the order $\rho^{5/2}$ are found to have at most two

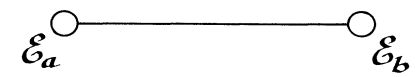

FIG. 4. The simplest Debye graph Π_D ($N=0, M_D=1$).

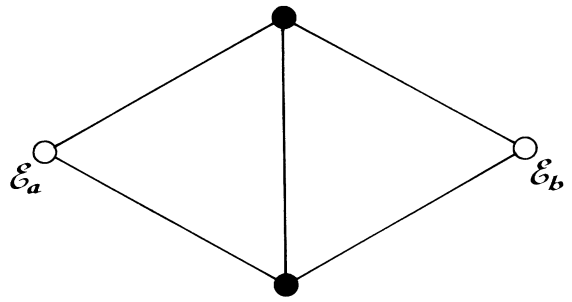

FIG. 5. The bare bridge graph Π_D ($N=2, M_D=5$).

bonds f_R (simple examples strongly suggest that all the remaining graphs with three or more bonds f_R are at least of order ρ^3). Taking into account the excluded-convolution rule as well as the parity of the measure $\mathcal{D}(\xi)\rho_g(\mathcal{E})$, which makes some contributions vanish, the graphs of interest can be listed as follows.

A. Debye graphs ($M_R=0, M_D'=0, M_D''=0$)

There are five graphs Π_D built only with bonds f_D that contribute: the simplest graph $\Pi_D(N=0, M_D=1)$ (see Fig. 4) and the bridge graphs shown in Figs. 5 and 6 (the bridges in Fig. 6 are built by convoluting the bridge in Fig. 5 with one or two bonds f_D).

Their contributions read

$$\frac{1}{2}\sum_{\alpha_a,\alpha_b}\beta_{ab}\int_0^1 dg\int \mathcal{D}(\xi_a)\mathcal{D}(\xi_b)\rho_g(\mathcal{E}_a)\rho_g(\mathcal{E}_b)\int d\mathbf{r}\frac{1}{r}[-g\beta_{ab}\exp(-g^{1/2}\kappa r)/r]=-\frac{1}{2}\sum_{a,b}\beta_{ab}\int_0^1 dg\,\rho_{\alpha_a}\rho_{\alpha_b}4\pi\beta_{ab}\kappa^{-1}g^{1/2}$$
$$=-\frac{\kappa^3}{12\pi} \tag{4.1}$$

for the familiar Debye graph,

$$\frac{1}{2}\sum_{\alpha_a\alpha_b\alpha_1\alpha_2}\beta_{ab}\int_0^1 dg\int \mathcal{D}(\xi_a)\mathcal{D}(\xi_b)\mathcal{D}(\xi_1)\mathcal{D}(\xi_2)\rho_g(\mathcal{E}_a)\rho_g(\mathcal{E}_b)\rho_g(\mathcal{E}_1)\rho_g(\mathcal{E}_2)$$
$$\times\int d\mathbf{r}\frac{1}{r}\int d\mathbf{r}_1 d\mathbf{r}_2\left[-g\beta_{a1}\frac{\exp(-g^{1/2}\kappa r_1)}{r_1}\right]\left[-g\beta_{1b}\frac{\exp(-g^{1/2}\kappa r_{1b})}{r_{1b}}\right]$$
$$\times\left[-g\beta_{a2}\frac{\exp(-g^{1/2}\kappa r_2)}{r_2}\right]\left[-g\beta_{2b}\frac{\exp(-g^{1/2}\kappa r_{2b})}{r_{2b}}\right]\left[-g\beta_{12}\frac{\exp(-g^{1/2}\kappa r_{12})}{r_{12}}\right]$$
$$=-\frac{1}{9}\int d\mathbf{x}\,d\mathbf{x}_1\,d\mathbf{x}_2\frac{1}{x}\frac{e^{-x_1}}{x_1}\frac{e^{-|\mathbf{x}_1-\mathbf{x}|}}{|\mathbf{x}_1-\mathbf{x}|}\frac{e^{-x_2}}{x_2}\frac{e^{-|\mathbf{x}_2-\mathbf{x}|}}{|\mathbf{x}_2-\mathbf{x}|}\frac{e^{-|\mathbf{x}_2-\mathbf{x}_1|}}{|\mathbf{x}_2-\mathbf{x}_1|}\sum_{\alpha\beta\gamma\delta}\beta^6 e_\alpha^3 e_\beta^3 e_\gamma^3 e_\delta^3\kappa^{-3}\rho_\alpha\rho_\beta\rho_\gamma\rho_\delta \tag{4.2}$$

for the bare bridge graph, and

$$-\frac{1}{9}\int d\mathbf{x}\,d\mathbf{x}_1\,d\mathbf{x}_2\left[\frac{e^{-x}}{x}-\frac{1}{x}-\frac{e^{-x}}{2}\right]\frac{e^{-x_1}}{x_1}\frac{e^{-|\mathbf{x}_1-\mathbf{x}|}}{|\mathbf{x}_1-\mathbf{x}|}\frac{e^{-x_2}}{x_2}\frac{e^{-|\mathbf{x}_2-\mathbf{x}|}}{|\mathbf{x}_2-\mathbf{x}|}\frac{e^{-|\mathbf{x}_2-\mathbf{x}_1|}}{|\mathbf{x}_2-\mathbf{x}_1|}\sum_{\alpha\beta\gamma\delta}\beta^6 e_\alpha^3 e_\beta^3 e_\gamma^3 e_\delta^3\kappa^{-3}\rho_\alpha\rho_\beta\rho_\gamma\rho_\delta \tag{4.3}$$

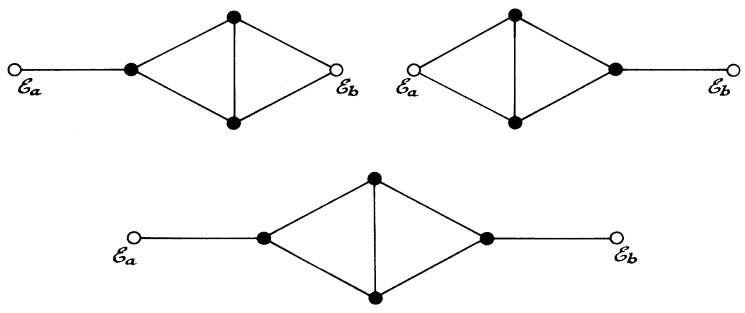

FIG. 6. The three graphs obtained by convoluting the bridge graph shown in Fig. 5 with one or two bonds f_D.

for the convoluted bridges. The contribution (4.1) of the simplest graph is nothing but the well-known classical Debye-Hückel term. In (4.2) and (4.3), the dimensionless integrals can be evaluated numerically by Legendre polynomial expansion. We stress that the contributions (4.1)–(4.3) are exactly proportional to half-integer powers of ρ. This is due to the fact that the functional integrations over the filament shapes exactly amount to replace each $\rho_g(\mathcal{E}_i)$ by the corresponding particle density ρ_{α_i}. This property holds for any Debye graph Π_D with only bonds f_D.

B. Diffraction graphs ($M_R=0$, $M_D'\neq 0$, or/and $M_D''\neq 0$)

The sole contributing diffraction graph $\Pi_{\rm dif}$ ($N=1, M_D=0, M_D'=2, M_D''=0$) has one internal point $\mathcal{E}_1$ linked to $\mathcal{E}_a$ and $\mathcal{E}_b$ by the bonds $\lambda_{\alpha_1}\xi_1\cdot\nabla_1 f_D(|\mathbf{r}_1-\mathbf{r}_a|)$ and $\lambda_{\alpha_1}\xi_1\cdot\nabla_1 f_D(|\mathbf{r}_1-\mathbf{r}_b|)$ (see Fig. 7).

Only the leading contribution of this graph has to be retained since it is of order $\rho^{5/2}$. It is obtained by replacing $\rho_g(\mathcal{E}_1)$ by ρ_{α_1} and reads

$$\frac{1}{2}\sum_{\alpha_a\alpha_b\alpha_1}\beta_{ab}\beta_{a1}\beta_{1b}\rho_{\alpha_a}\rho_{\alpha_b}\rho_{\alpha_1}\lambda_{\alpha_1}^2\frac{1}{\kappa}\int_0^1 dg\, g^{3/2}\int d\mathbf{x}\,d\mathbf{x}_1\frac{1}{x}\int\mathcal{D}(\xi_1)\int_0^1 ds\int_0^1 dt\left[\xi_1(s)\cdot\nabla_{\mathbf{x}_1}\frac{e^{-x_1}}{x_1}\right]\left[\xi_1(t)\cdot\nabla_{\mathbf{x}_1}\frac{e^{-|\mathbf{x}_1-\mathbf{x}|}}{|\mathbf{x}_1-\mathbf{x}|}\right]$$

$$=\frac{1}{60}\sum_{\alpha_1}\beta e_{\alpha_1}^2\rho_{\alpha_1}\lambda_{\alpha_1}^2\frac{\kappa^4}{(4\pi)^2}\frac{1}{\kappa}\frac{1}{(2\pi)^3}\int d\mathbf{u}\frac{4\pi}{u^2}\left[\frac{-4\pi i\mathbf{u}}{u^2+1}\right]\cdot\left[\frac{4\pi i\mathbf{u}}{u^2+1}\right]=\frac{1}{120}\sum_{\alpha}\beta e_\alpha^2\lambda_\alpha^2\kappa^3\rho_\alpha\,, \tag{4.4}$$

where we have used the covariance (2.2) of the Gaussian measure $\mathcal{D}(\xi)$, Fourier-Plancherel identity, and $\int_0^\infty du\, u^2/(u^2+1)^2=\pi/4$. In the following cases, there proves to be no other diagram with $\lambda_{\alpha_i}\xi_i\cdot\nabla_i f_D$ bonds and/or $f_{\rm dip}$ bonds that contributes to the order $\rho^{5/2}$.

C. Chain graphs with one f_R bond

(i) First we consider the simple graph Π_R ($N=0, M_R=1$) with only one bond $f_R(\mathcal{E}_a,\mathcal{E}_b)$ (see Fig. 8). The leading contribution of this graph is of order ρ^2 and is obtained by replacing f_R by either f_T or $f_D^2/2$ in the scaling decomposition (3.7), and $\rho_g(\mathcal{E}_a)$ ($\rho_g(\mathcal{E}_b)$) by ρ_{α_a} (ρ_{α_b}). In fact, each of the two graphs $G_\Pi^{\rm scaled}$ built with f_T or $f_D^2/2$ gives a divergent contribution to the free energy because of a spurious singularity at the origin. In accordance with the general arguments exposed in Sec. III B, this nonphysical divergency is removed by merely adding both contributions. The finite total contribution of these two graphs can then be calculated as

$$\frac{1}{2}\sum_{\alpha_a\alpha_b}\beta_{ab}\rho_{\alpha_a}\rho_{\alpha_b}\int_0^1 dg\lim_{R\to\infty}\int_{r<R}d\mathbf{r}\frac{1}{r}\left\{(2\pi\lambda_{\alpha_a\alpha_b}^2)^{3/2}\langle\mathbf{r}|\exp(-\beta h^g_{\alpha_a\alpha_b})|\mathbf{r}\rangle-1+\frac{g\beta_{ab}}{r}-\frac{g^2\beta_{ab}^2}{2}\left[\frac{1-\exp(-2g^{1/2}\kappa r)}{r^2}\right]\right\}$$

$$=-\frac{1}{2}\sum_{\alpha_a\alpha_b}\rho_{\alpha_a}\rho_{\alpha_b}\lim_{R\to\infty}\left\{\frac{\beta_{ab}^3}{2}\int_0^1 dg\, g^2 4\pi\int_0^{2g^{1/2}\kappa R}dx\frac{(1-e^{-x})}{x}\right.$$

$$\left.+\int_{r<R}d\mathbf{r}\left[(2\pi\lambda_{\alpha_a\alpha_b}^2)^{3/2}\langle\mathbf{r}|\exp(-\beta h_{\alpha_a\alpha_b})|\mathbf{r}\rangle-1+\frac{\beta_{ab}}{r}-\frac{\beta_{ab}^2}{2r^2}\right]\right\}+\frac{\pi}{6}\sum_{\alpha_a\alpha_b}\beta_{ab}\lambda_{\alpha_a\alpha_b}^2\rho_{\alpha_a}\rho_{\alpha_b}$$

$$=-\frac{1}{2}\sum_{\alpha\beta}\rho_\alpha\rho_\beta\lim_{R\to\infty}\left\{\int_{r<R}d\mathbf{r}\left[(2\pi\lambda_{\alpha\beta}^2)^{3/2}\langle\mathbf{r}|\exp(-\beta h_{\alpha\beta})|\mathbf{r}\rangle-1+\frac{\beta e_\alpha e_\beta}{r}-\frac{\beta^2e_\alpha^2e_\beta^2}{2r^2}\right]+\frac{2\pi}{3}\beta^3e_\alpha^3e_\beta^3\ln(\kappa R)\right\}$$

$$-\frac{\pi}{3}(C+\ln 2-\tfrac{1}{6})\sum_{\alpha\beta}\beta^3e_\alpha^3e_\beta^3\rho_\alpha\rho_\beta\,, \tag{4.5}$$

where $h^g_{\alpha\beta}$ is the one-body Coulomb Hamiltonian of the relative particle with reduced mass $m_\alpha m_\beta/(m_\alpha+m_\beta)$ in the potential $ge_\alpha e_\beta/r$ ($h^{g=1}_{\alpha\beta}=h_{\alpha\beta}$), and $\lambda_{\alpha\beta}$ is the corresponding thermal de Broglie wavelength (C is Euler-Mascheroni's constant). The matrix elements of $\exp(-\beta h^g_{\alpha\beta})$ are introduced by applying backwards the Feynman-Kac formula [3] and by factoring out the trivial kinetic contribution of the center of mass, i.e.,

$$\int\mathcal{D}(\xi_a)\mathcal{D}(\xi_b)\exp\left[-\beta g e_{\alpha_a}e_{\alpha_b}\int_0^1 ds\, v_c(|\mathbf{r}+\lambda_{\alpha_b}\xi_b(s)-\lambda_{\alpha_a}\xi_\alpha(s)|)\right]$$

$$=(2\pi\lambda_{\alpha_a}^2)^{3/2}(2\pi\lambda_{\alpha_b}^2)^{3/2}\langle\mathbf{0r}|\exp\left\{-\beta\left[-\frac{\hbar^2}{2m_{\alpha_a}}\Delta_a-\frac{\hbar^2}{2m_{\alpha_b}}\Delta_b+\frac{ge_\alpha e_\beta}{r_{ab}}\right]\right\}|\mathbf{0r}\rangle$$

$$=(2\pi\lambda_{\alpha_a\alpha_b}^2)^{3/2}\langle\mathbf{r}|\exp(-\beta h^g_{\alpha_a\alpha_b})|\mathbf{r}\rangle\,.$$

In the first line of (4.5), the introduction of $\lim_{R\to\infty}$ is just a mathematical trick (the integral does converge). The second line is obtained through the identity (A13) derived in the Appendix. This identity is a suitable extension to the Coulomb case of the usual differentiation trace identity

$$(\partial/\partial g)\mathrm{Tr}[\exp(-\beta(h_0+gV_{\mathrm{int}}))-\exp(-\beta h_0)]=-\beta\,\mathrm{Tr}[V_{\mathrm{int}}\exp(-\beta(h_0+gV_{\mathrm{int}}))]\ ,$$

valid for any integrable potential V_{int} (h_0 is the kinetic Hamiltonian). The long-range part of the Coulomb potential gives rise to the last additional term in the second line of (4.5). It turns out that this term vanishes because of the neutrality condition. In the third line of (4.5) the logarithmic divergency when $R\to\infty$ of the truncated trace of $\exp(-\beta h_{\alpha\beta})$ and the logarithmic term $(2\pi/3)\beta^3 e_\alpha^3 e_\beta^3 \ln(\kappa R)$ cancel out, as it should be. The resulting quantity $\lim_{R\to\infty}$ takes the form $\mathrm{Const}\times\ln(\mathrm{Const}\times\kappa)$ where the involved "constants" depend on the temperature and are built with the Landau and de Broglie lengths, i.e., $\beta e_\alpha e_\beta$ and $\lambda_{\alpha\beta}$.

The next contribution of order $\rho^{5/2}$ of Π_R ($N=0, M_R=1$) is given by the mixed function $\kappa H_1(x) f_T$ and by the κ-scaled function $\kappa^3\beta_{ab}^3[1-\exp(-3x)]/6x^3$ in (3.7). It can be expressed as

$$\begin{aligned}
&\tfrac{1}{2}\sum_{\alpha_a\alpha_b}\beta_{ab}\rho_{\alpha_a}\rho_{\alpha_b}\int_0^1 dg\int d\mathbf{r}\,\frac{1}{r}\left\{g\frac{\beta_{ab}}{r}[1-\exp(-g^{1/2}\kappa r)]\left[(2\pi\lambda^2_{\alpha_a\alpha_b})^{3/2}\langle\mathbf{r}|\exp(-\beta h^g_{\alpha_a\alpha_b})|\mathbf{r}\rangle-1+\frac{g\beta_{ab}}{r}\right]\right.\\
&\qquad\left.-\frac{g^3\beta_{ab}^3}{2r^3}[1-\exp(-g^{1/2}\kappa r)]+\frac{g^3\beta_{ab}^3}{6r^3}[1-\exp(-3g^{1/2}\kappa r)]\right\}\\
&=\tfrac{1}{2}\sum_{\alpha_a\alpha_b}\beta_{ab}\rho_{\alpha_a}\rho_{\alpha_b}\left\{\int_0^1 dg\int d\mathbf{r}\,g\frac{\beta_{ab}}{r}[1-\exp(-g^{1/2}\kappa r)]\frac{1}{r}\left[(2\pi\lambda_{\alpha_a\alpha_b})^{3/2}\langle\mathbf{r}|\exp(-\beta h^g_{\alpha_a\alpha_b})|\mathbf{r}\rangle-1+\frac{g\beta_{ab}}{r}\right]\right.\\
&\qquad\left.-\kappa\frac{\beta_{ab}^3}{6}\int_0^1 dg\,g^{7/2}4\pi\int_0^\infty dx\frac{(1-e^{-x})(2-e^{-x}-e^{-2x})}{x^2}\right\}.
\end{aligned}\tag{4.6}$$

The integral $\int d\mathbf{r}$ in the right-hand side of (4.6) can be rewritten as the sum of $\int_{r<R}d\mathbf{r}$ and $\int_{R<r}d\mathbf{r}$ for any given R. By choosing R large enough compared to $\beta e_{\alpha_a}e_{\alpha_b}$, λ_{α_a}, and λ_{α_b}, we can replace $\int_{R<r}d\mathbf{r}$ by

$$\int_{R<r}d\mathbf{r}\,g\frac{\beta_{ab}}{r}[1-\exp(-g^{1/2}\kappa r)]\frac{g^2\beta_{ab}^2}{2r^3}=2\pi g^{7/2}\kappa\beta_{ab}^3\int_{g^{1/2}\kappa R}^\infty dx\frac{(1-e^{-x})}{x^2}\ ,\tag{4.7}$$

disregarding terms that go to zero when $R\to\infty$ uniformly with respect to κ. In the integral $\int_{r<R}d\mathbf{r}$, we can first replace $g\beta_{ab}[1-\exp(-g^{1/2}\kappa r)]/r$ by $g^{3/2}\kappa\beta_{ab}$ and then proceed to an integration by parts over g by using the differentiation trace identity (A13). The resulting expression for the term of order $\rho^{5/2}$ in the contribution (4.6) then reads

$$\begin{aligned}
&-\tfrac{1}{2}\sum_{\alpha\beta}\beta e_\alpha e_\beta\kappa\rho_\alpha\rho_\beta\lim_{R\to\infty}\left\{\frac{2\pi}{3}\beta^3 e_\alpha^3 e_\beta^3\ln(\kappa R)+\int_{r<R}d\mathbf{r}\left[(2\pi\lambda^2_{\alpha\beta})^{3/2}\langle\mathbf{r}|\exp(-\beta h_{\alpha\beta})|\mathbf{r}\rangle-1+\frac{\beta e_\alpha e_\beta}{r}-\frac{\beta^2 e_\alpha^2 e_\beta^2}{2r^2}\right]\right\}\\
&+\tfrac{1}{30}\sum_\alpha\beta e_\alpha^2\lambda_\alpha^2\kappa^3\rho_\alpha+\frac{2\pi}{9}(\tfrac{10}{9}-C-\ln 3)\sum_{\alpha\beta}\beta^4 e_\alpha^4 e_\beta^4\kappa\rho_\alpha\rho_\beta\\
&+\tfrac{3}{4}\sum_{\alpha\beta}\beta e_\alpha e_\beta\kappa\rho_\alpha\rho_\beta\int_0^1 dg\,g^{1/2}\lim_{R\to\infty}\left\{\frac{2\pi}{3}g^3\beta^3 e_\alpha^3 e_\beta^3\ln(\kappa R)+\int_{r<R}d\mathbf{r}\left[(2\pi\lambda^2_{\alpha\beta})^{3/2}\langle\mathbf{r}|\exp(-\beta h^g_{\alpha\beta})|\mathbf{r}\rangle\right.\right.\\
&\qquad\left.\left.-1+\frac{g\beta e_\alpha e_\beta}{r}-\frac{g^2\beta^2 e_\alpha^2 e_\beta^2}{2r^2}\right]\right\}.
\end{aligned}\tag{4.8}$$

(ii) We turn now to the contributions of the chain graphs Π_{chain} with one bond f_R and one or two bonds f_D, i.e., the three graphs shown in Fig. 9. The leading contributions of these graphs are associated to the graphs $G^{\mathrm{scaled}}_{\Pi,\min}$ arising from the replacement of f_R by $f_D^2/2$. The total contribution of the latter graphs is of order ρ^2 and can be calculated as

$$\frac{1}{2}\sum_{\alpha_a\alpha_b}\beta_{ab}\rho_{\alpha_a}\rho_{\alpha_b}\int_0^1 dg\, g^2\int d\mathbf{x}\frac{1}{x}\left\{-\frac{2}{\kappa^2}\sum_{\alpha_1}\rho_{\alpha_1}\beta_{a1}\beta_{1b}^2\int d\mathbf{x}_1\frac{e^{-x_1}}{x_1}\frac{e^{-2|\mathbf{x}_1-\mathbf{x}|}}{2|\mathbf{x}_1-\mathbf{x}|^2}\right.$$
$$\left.+\frac{1}{\kappa^4}\sum_{\alpha_1\alpha_2}\rho_{\alpha_1}\rho_{\alpha_2}\beta_{a1}\beta_{12}^2\beta_{1b}\int d\mathbf{x}_1\, d\mathbf{x}_2\frac{e^{-x_1}}{x_1}\frac{e^{-2|\mathbf{x}_1-\mathbf{x}_2|}}{2|\mathbf{x}_1-\mathbf{x}_2|^2}\frac{e^{-|\mathbf{x}_2-\mathbf{x}|}}{|\mathbf{x}_2-\mathbf{x}|}\right\}$$
$$=\frac{1}{24\pi}\sum_{\alpha\beta}\beta^3e_\alpha^3e_\beta^3\rho_\alpha\rho_\beta\left\{-\frac{1}{(2\pi)^3}\int d\mathbf{u}\frac{4\pi}{u^2}\frac{4\pi}{(1+u^2)}\frac{4\pi}{u}\arctan\left[\frac{u}{2}\right]\right.$$
$$\left.+\frac{1}{8\pi}\frac{1}{(2\pi)^3}\int d\mathbf{u}\frac{4\pi}{u^2}\left[\frac{4\pi}{(1+u^2)}\right]^2\frac{4\pi}{u}\arctan\left[\frac{u}{2}\right]\right\}$$
$$=\frac{\pi}{3}(\ln 2-\ln 3-\tfrac{1}{6})\sum_{\alpha\beta}\beta^3e_\alpha^3e_\beta^3\rho_\alpha\rho_\beta\,, \tag{4.9}$$

where we have used the Fourier-Plancherel identity together with the convolution theorem [$(4\pi/u)\arctan(u/2)$ is the Fourier transform of $\exp(-2x)/x^2$].

The next contributions of the above chain graphs are of order $\rho^{5/2}$ and arise either from the κ-scaled term $\kappa^3\beta_{ij}^3[1-\exp(-3x)]/6x^3$ or from f_T in the scaling decomposition (3.7) of f_R (here the term of order κ^3 linear in the ξ's does not give any contribution for parity reasons). The contributions associated to the κ-scaled term can be again calculated along similar lines to (4.9) by using the Fourier transform of $[1-\exp(-3x)]/x^3$, which is $4\pi[(\frac{1}{2})\ln((9+u^2)/u^2)+(3/u)\arctan(u/3)]$. Their sum is equal to

$$\frac{\pi}{9}(2\ln 3-3\ln 4)\sum_{\alpha\beta}\beta^4e_\alpha^4e_\beta^4\kappa\rho_\alpha\rho_\beta\,. \tag{4.10}$$

For calculating the contributions of order $\rho^{5/2}$ associated to the decomposed graphs with f_T in place of f_R, we can replace $\rho(\mathcal{C}_i)$ by ρ_{α_i}. Since these decomposed graphs have a chain structure, their total contribution can be easily expressed in Fourier space as

$$-\frac{1}{\pi}\sum_{\alpha\beta}\beta e_\alpha e_\beta\kappa\rho_\alpha\rho_\beta\int_0^1 dg\, g^{1/2}\int_0^\infty du\,\tilde{f}_{T,\alpha\beta}^g(g^{1/2}\kappa u)\left[\frac{2}{(1+u^2)}-\frac{1}{(1+u^2)^2}\right], \tag{4.11}$$

with

$$\tilde{f}_{T,\alpha\beta}^g(k)=\int d\mathbf{r}\exp(i\mathbf{k}\cdot\mathbf{r})\left[(2\pi\lambda_{\alpha\beta}^2)^{3/2}\langle\mathbf{r}|\exp(-\beta h_{\alpha\beta}^g)|\mathbf{r}\rangle-1+\frac{g\beta e_\alpha e_\beta}{r}-\frac{g^2\beta^2e_\alpha^2e_\beta^2}{2r^2}\right]. \tag{4.12}$$

When $k\to 0$, $\tilde{f}_{T,\alpha\beta}^g(k)$ diverges logarithmically as

$$\tilde{f}_{T,\alpha\beta}^g(k)=\lim_{R\to\infty}\left\{\int_{r<R}d\mathbf{r}\left[(2\pi\lambda_{\alpha\beta}^2)^{3/2}\langle\mathbf{r}|\exp(-\beta h_{\alpha\beta}^g)|\mathbf{r}\rangle-1+\frac{g\beta e_\alpha e_\beta}{r}-\frac{g^2\beta^2e_\alpha^2e_\beta^2}{2r^2}\right]+\frac{2\pi}{3}g^3\beta^3e_\alpha^3e_\beta^3\ln(kR)\right\}$$
$$-\frac{2\pi g^3}{3}\beta^3e_\alpha^3e_\beta^3(1-C)+o(1)\,. \tag{4.13}$$

The resulting low-density behavior of (4.11) follows by inserting (4.13) with $k=g^{1/2}\kappa u$, and reads at the order $\rho^{5/2}$

$$\frac{\pi}{9}(\tfrac{7}{9}-C)\sum_{\alpha\beta}\beta^4e_\alpha^4e_\beta^4\kappa\rho_\alpha\rho_\beta-\tfrac{3}{4}\sum_{\alpha\beta}\beta e_\alpha e_\beta\kappa\rho_\alpha\rho_\beta\int_0^1 dg\, g^{1/2}\lim_{R\to\infty}\left\{\int_{r<R}d\mathbf{r}\left[(2\pi\lambda_{\alpha\beta}^2)^{3/2}\langle\mathbf{r}|\exp(-\beta h_{\alpha\beta}^g)|\mathbf{r}\rangle-1\right.\right.$$
$$\left.\left.+\frac{g\beta e_\alpha e_\beta}{r}-\frac{g^2\beta^2e_\alpha^2e_\beta^2}{2r^2}\right]+\frac{2\pi}{3}g^3\beta^3e_\alpha^3e_\beta^3\ln(\kappa R)\right\}, \tag{4.14}$$

where we have used $\int_0^\infty du\,(\ln u)[2/(1+u^2)-1/(1+u^2)^2]=\pi/4$ and $\int_0^\infty du[2/(1+u^2)]-1/(1+u^2)^2]=3\pi/4$.

D. Loop graphs with one f_R bond

The two simplest loop graphs with one f_R bond and two f_D bonds are shown in Figs. 10(a) and 10(b). Their leading contributions are of order $\rho^{5/2}$ and are obtained by replacing f_R by $f_D^2/2$. Using the Fourier-Plancherel identity and the convolution theorem, we find that the sum of these contributions reads

$$\frac{32\pi}{9}\int_0^\infty du \frac{1}{(1+u^2)} \arctan\left[\frac{u}{2}\right] \arctan(u) \sum_{\alpha\beta\gamma} \beta^5 e_\alpha^3 e_\beta^4 e_\gamma^3 \kappa^{-1} \rho_\alpha \rho_\beta \rho_\gamma \ . \tag{4.15}$$

The loop graphs shown in Fig. 11 are obtained by convoluting the graphs in Figs. 10(a) and 10(b) with one or two bonds f_D. Their total leading contribution is also of order $\rho^{5/2}$ and reads

$$\frac{32\pi}{9}\int_0^\infty du \frac{1}{(u^2+1)} \arctan\left[\frac{u}{2}\right] \left[\arctan\left[\frac{u}{2}\right] - \arctan(u) - \frac{u}{2(u^2+4)}\right] \sum_{\alpha\beta\gamma} \beta^5 e_\alpha^3 e_\beta^4 e_\gamma^3 \kappa^{-1} \rho_\alpha \rho_\beta \rho_\gamma \ . \tag{4.16}$$

The loop graph with three bonds f_D shown in Fig. 12 also gives a leading contribution of order $\rho^{5/2}$, i.e.,

$$-\frac{64\pi^2}{9}\int_0^\infty du \frac{1}{(1+u^2)^2} \arctan\left[\frac{u}{2}\right] \arctan(u) \sum_{\alpha\beta\gamma\delta} \beta^6 e_\alpha^3 e_\beta^3 e_\gamma^3 e_\delta^3 \kappa^{-1} \rho_\alpha \rho_\beta \rho_\gamma \rho_\delta \ , \tag{4.17}$$

as well as the three other graphs obtained by convolutions with one or two bonds f_D (see Fig. 13), the total contribution of which reads

$$\frac{64\pi^2}{9}\int_0^\infty du \frac{1}{(u^2+1)^2} \arctan\left[\frac{u}{2}\right] \left[\arctan(u) - \arctan\left[\frac{u}{2}\right] + \frac{u}{2(u^2+4)}\right] \sum_{\alpha\beta\gamma\delta} \beta^6 e_\alpha^3 e_\beta^3 e_\gamma^3 e_\delta^3 \kappa^{-3} \rho_\alpha \rho_\beta \rho_\gamma \rho_\delta \ . \tag{4.18}$$

E. Chain graphs with two f_R bonds

The corresponding graphs are built with two bonds f_R and at most three bonds f_D. These graphs are shown in Figs. 14–17. Their leading contributions are of order $\rho^{5/2}$ and arise from the replacement of the two bonds f_R by $f_D^2/2$. After use of the convolution theorem in Fourier space, they can be rewritten as

$$-\frac{32\pi^2}{9}\int_0^\infty du \left[\frac{1}{u}\arctan\left[\frac{u}{2}\right]\right]^2 \frac{1}{(1+u^2)} \left[1 - \frac{2}{(1+u^2)} + \frac{1}{(1+u^2)^2}\right] \sum_{\alpha\beta\gamma\delta} \beta^6 e_\alpha^3 e_\beta^3 e_\gamma^3 e_\delta^3 \kappa^{-3} \rho_\alpha \rho_\beta \rho_\gamma \rho_\delta \tag{4.19}$$

for the four graphs shown in Figs. 14 and 15, and

$$\frac{8\pi}{9}\int_0^\infty du \left[\frac{1}{u}\arctan\left[\frac{u}{2}\right]\right]^2 \left[1 - \frac{2}{(1+u^2)} + \frac{1}{(1+u^2)^2}\right] \sum_{\alpha\beta\gamma} \beta^5 e_\alpha^3 e_\beta^4 e_\gamma^3 \kappa^{-1} \rho_\alpha \rho_\beta \rho_\gamma \tag{4.20}$$

for the four remaining graphs shown in Figs. 16 and 17.

F. Final results and comments

The final expression of the excess free-energy density at the order $\rho^{5/2}$ is obtained by summing the contributions [(4.1)–(4.5), (4.8)–(4.10), and (4.14)–(4.20)] with the result

$$\begin{aligned}
\frac{\beta F}{\Lambda} - \frac{\beta F_{\rm id}}{\Lambda} = & -\frac{\kappa^3}{12\pi} - \frac{\pi}{3}(C+\ln 3) \sum_{\alpha,\beta} \beta^3 e_\alpha^3 e_\beta^3 \rho_\alpha \rho_\beta \\
& - \tfrac{1}{2} \sum_{\alpha,\beta} \rho_\alpha \rho_\beta \lim_{R\to\infty} \left\{ \int_{r<R} d\mathbf{r} \left[(2\pi\lambda_{\alpha\beta}^2)^{3/2} \langle \mathbf{r}|\exp(-\beta h_{\alpha\beta})|\mathbf{r}\rangle - 1 + \frac{\beta e_\alpha e_\beta}{r} - \frac{\beta^2 e_\alpha^2 e_\beta^2}{2r^2} \right] + \frac{2\pi}{3} \beta^3 e_\alpha^3 e_\beta^3 \ln(\kappa R) \right\} \\
& + \frac{\pi}{3}(1-C-2\ln 2) \sum_{\alpha,\beta} \beta^4 e_\alpha^4 e_\beta^4 \kappa \rho_\alpha \rho_\beta + \tfrac{2}{3} C_1 \sum_{\alpha,\beta,\gamma} \beta^5 e_\alpha^3 e_\beta^4 e_\gamma^3 \kappa^{-1} \rho_\alpha \rho_\beta \rho_\gamma \\
& + \tfrac{2}{3} C_2 \sum_{\alpha,\beta,\gamma,\delta} \beta^6 e_\alpha^3 e_\beta^3 e_\gamma^3 e_\delta^3 \kappa^{-3} \rho_\alpha \rho_\beta \rho_\gamma \rho_\delta + \tfrac{1}{24} \sum_\alpha \frac{\beta^2 \hbar^2 e_\alpha^2}{m_\alpha} \kappa^3 \rho_\alpha \\
& - \tfrac{1}{2} \sum_{\alpha,\beta} \beta e_\alpha e_\beta \kappa \rho_\alpha \rho_\beta \lim_{R\to\infty} \left\{ \int_{r<R} d\mathbf{r} \left[(2\pi\lambda_{\alpha\beta}^2)^{3/2} \langle \mathbf{r}|\exp(-\beta h_{\alpha\beta})|\mathbf{r}\rangle - 1 + \frac{\beta e_\alpha e_\beta}{r} - \frac{\beta^2 e_\alpha^2 e_\beta^2}{2r^2} \right] \right. \\
& \left. + \frac{2\pi}{3} \beta^3 e_\alpha^3 e_\beta^3 \ln(\kappa R) \right\} + O(\rho^3 \ln \rho) \ ,
\end{aligned} \tag{4.21}$$

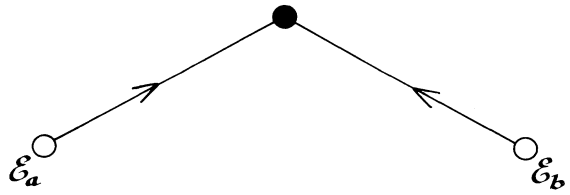

FIG. 7. The diffraction graph Π_{diff} ($N=1, M_D'=2$). The solid lines with an arrow represent bonds $\lambda_{\alpha_i}\xi_i\cdot\nabla_i f_D$ (the arrow indicates the point i on which acts the gradient).

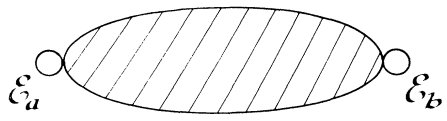

FIG. 8. The graph Π_R ($N=0, M_R=1$).

where the pure constants C_1 and C_2 have been estimated by numerical evaluations of the dimensionless integrals involved in [(4.2), (4.3), and (4.15)–(4.20)] as $C_1 \simeq 15.201\pm0.001$ and $C_2 \simeq -14.734\pm0.001$ [28]. All the graphs G_{Π}^{scaled} that contribute to (4.21) are represented in Fig. 18.

The truncated expansion (4.21) does exhibit the structure (3.12) obtained from the general qualitative analysis of Sec. III B. The various terms can be associated to specific physical effects. The purely classical terms "à la Debye" arise from graphs G_{Π}^{scaled} built with only κ-scaled bonds independent of the shapes of the filaments. Consequently, they can be viewed as long-range contributions of the classical part of the interactions screened with the Debye length κ^{-1}. The term of order $\rho^{5/2}$ exactly proportional to $\hbar^2$ is of the diffraction type in the sense that it describes quantum corrections to a classical treatment of the long-range part of the interactions. These quantum effects are associated to multipolelike interactions between the filaments, which enter in shape-dependent bonds like f_T or $\lambda_{\alpha_i}\xi_i\cdot\nabla_i f_D$, for instance. Note, in particular, that both graphs Π_R ($N=0, M_R=1$) [with $\kappa H_1(x) f_T$ in place of f_R] and the purely diffraction graph Π_{diff} ($N=1, M_D=0, M_D'=2, M_D''=0$) contribute to the above diffraction term of order $\rho^{5/2}$, as shown by Eq. (4.8) and (4.4), respectively. We stress that the presence of these diffraction terms shows that the interactions cannot be entirely treated at a classical level at large distances. Eventually, there are terms that involve truncated traces of the quantum Gibbs factor for a finite number of charges. They describe short-range quantum effects and take into account the contributions of both bound and scattering states. They arise from graphs G_{Π}^{scaled} made with at least one function f_T. Here, at the present order $\rho^{5/2}$, it turns out that the short-range quantum contributions can be entirely expressed in terms of the one-body density matrix $\langle \mathbf{r}|\exp(-\beta h_{\alpha\beta})|\mathbf{r}\rangle$ [the last terms of (4.8) and (4.14), which are related to nontrivial integrals over g of $\langle \mathbf{r}|\exp(-\beta h_{\alpha\beta}^{g})|\mathbf{r}\rangle$, cancel out]. Such simplifications in favor of few-body density matrices calculated at $g=1$ only, might no longer occur at higher orders [in particular because of the functional dependence of $\rho_g(\mathcal{E})$, which has then to be taken into account].

At the order ρ^2, the above physical effects are completely disentangled. At higher orders, they may be coupled together in graphs G_{Π}^{scaled} involving simultaneously classical κ-scaled bonds, purely diffraction bonds (with a polynomial dependence in the ξ's) and the truncated bonds f_T. These graphs describe the many-body screening effects on the quantum states with a finite number of charges. It turns out that the quantum aspect of these collective phenomena can be treated perturbatively, as shown by the occurrence of the classical and diffraction bonds. Physically, this is due to the fact that the charges belonging to the screening clouds behave almost classically, i.e., their de Broglie wavelength becomes small compared to their relative distances in the low-density limit. The previous coupling mechanism appears already at the order $\rho^{5/2}$, and is illustrated by the term involving the truncated trace of $\exp(-\beta h_{\alpha\beta})$.

G. Comparisons and checkings

At the order ρ^2, we recover exactly the MB part of the expressions computed by Ebeling *et al.* [16,17]. For instance, the truncated trace of $\exp(-\beta h_{\alpha\beta})$, i.e., $\lim_{R\to\infty}\int d\mathbf{r}$ is nothing but the second virial quantum coefficient first introduced by Ebeling. All our terms of order $\rho^{5/2}$ do coincide with those determined from the effective-potential method, except the purely diffraction term

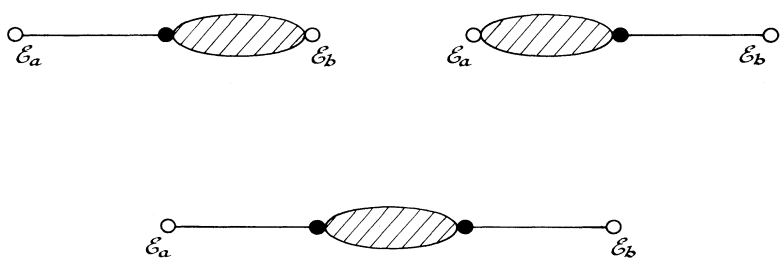

FIG. 9. The three chain graphs obtained by convoluting the graph Π_R shown in Fig. 8 with one or two bonds f_D.

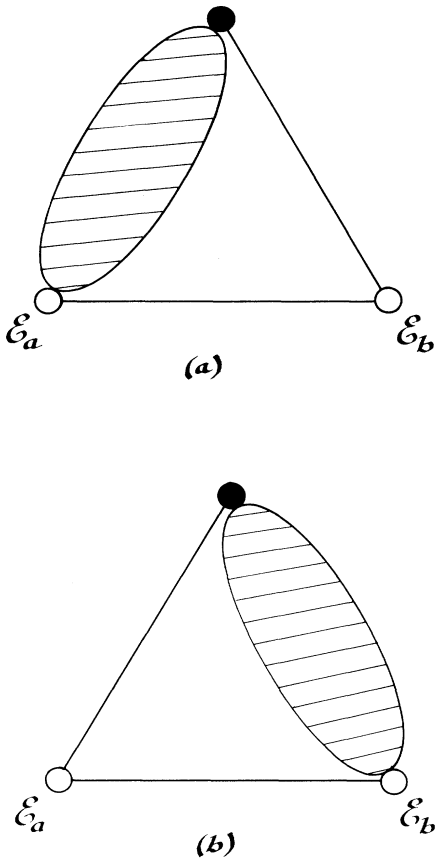

FIG. 10. (a) The "left" loop graph $\Pi^{(a)}_{\text{loop}}$ ($N=1, M_R=1$, $M_D=2$). (b) The "right" loop graph $\Pi^{(b)}_{\text{loop}}$ ($N=1, M_R=1$, $M_D=2$).

$$\frac{1}{24}\sum_{\alpha}\frac{\beta^2\hbar^2 e_\alpha^2}{m_\alpha}\kappa^3\rho_\alpha \ . \tag{4.22}$$

In this method, the term (4.22) arises in part [29] from the three-body effective interactions, which decay slowly for large triangular configurations [18]. The collective screening of these long-range interactions leads to contributions that are of order $\rho^{5/2}$ instead of ρ^3 (a similar mechanism makes the Debye correction be of order $\rho^{3/2}$ instead of ρ^2).

By specifying (4.21) to the case of the classical one-component plasma, we do recover the result of Cohen and Murphy [20]. Moreover, the first quantum correction to this classical expression can be obtained by expanding the truncated trace of $\exp(-\beta h_{\alpha\alpha})$ in powers of $\hbar$. It reduces to

$$\frac{\pi\beta^2 e^2\rho^2\hbar^2}{6m} \ , \tag{4.23}$$

which is nothing but the well-known $\hbar^2$ correction calculated by the Wigner-Kirkwood method [19]. Since this $\hbar^2$ correction is exactly proportional to ρ^2, the $\hbar^2$ contributions of all the virial coefficients of order larger than ρ^2 must vanish. This remarkable property is indeed satisfied by our $\rho^{5/2}$ coefficient, because of the presence of the diffraction term (4.22), which cancels the $\hbar^2$ contribution of

$$-\tfrac{1}{2}\beta e^2\kappa\rho^2 \lim_{R\to\infty}\int_{r<R} d\mathbf{r}\cdots \ .$$

Eventually, by using the β expansions of the truncated traces of $\exp(-\beta h_{\alpha\beta})$ [17], we have checked that the high-temperature form of (4.21) up to order $\beta^{5/2}$ do reduce to the MB part of the expressions derived by De Witt [24].

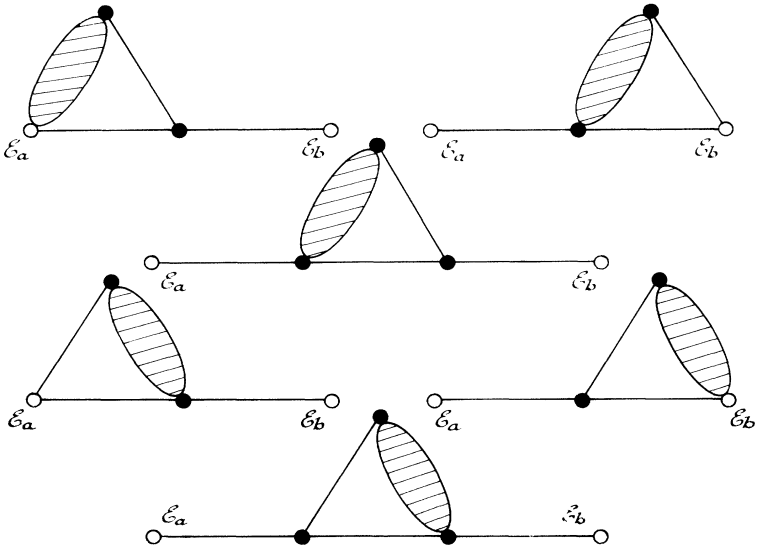

FIG. 11. The six graphs obtained by convoluting the loop graphs shown in Figs. 10(a) and 10(b) with one or two bonds f_D.

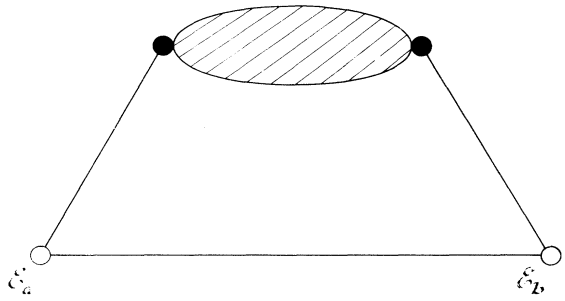

FIG. 12. The loop graph Π_{loop} ($N=2, M_R=1, M_D=3$).

V. EVALUATION OF THE PRESSURE AND OF THE OTHER THERMODYNAMIC FUNCTIONS

The virial expansion of any thermodynamic function can be inferred from (4.21) by using thermodynamic identities. The quantities that are related to the free energy via partial differentiations with respect to the density are the most easy to calculate because of the simple polynomial and logarithmic structure in the densities of (4.21). In particular, the pressure is calculated by inserting (4.21) in the thermodynamic relation

$$\beta P=\sum_\alpha \rho_\alpha \frac{\partial}{\partial \rho_\alpha}\left[\frac{\beta F}{\Lambda}\right]\Bigg|_\beta - \frac{\beta F}{\Lambda} \ . \tag{5.1}$$

Since κ is a homogeneous function of the ρ_α's of order $\frac{1}{2}$,

$$\sum_\alpha \rho_\alpha \frac{\partial}{\partial \rho_\alpha}\kappa=\tfrac{1}{2}\kappa \ , \tag{5.2}$$

$$\sum_\alpha \rho_\alpha \frac{\partial}{\partial \rho_\alpha}\ln(\text{const}\times\kappa)|_\beta=\tfrac{1}{2} \ , \tag{5.3}$$

and we find

$$\beta P=\sum_\alpha \rho_\alpha-\frac{\kappa^3}{24\pi}-\frac{\pi}{3}(\tfrac{1}{2}+C+\ln 3)\sum_{\alpha,\beta}\beta^3 e_\alpha^3 e_\beta^3 \rho_\alpha\rho_\beta-\tfrac{1}{2}\sum_{\alpha,\beta}\rho_\alpha\rho_\beta \lim_{R\to\infty}\{\ \}+\pi\left[\tfrac{1}{3}-\frac{C}{2}-\ln 2\right]\sum_{\alpha,\beta}\beta^4 e_\alpha^4 e_\beta^4 \kappa\rho_\alpha\rho_\beta$$

$$+C_1\sum_{\alpha,\beta,\gamma}\beta^5 e_\alpha^3 e_\beta^4 e_\gamma^3 \kappa^{-1}\rho_\alpha\rho_\beta\rho_\gamma+C_2\sum_{\alpha,\beta,\gamma,\delta}\beta^6 e_\alpha^3 e_\beta^3 e_\gamma^3 e_\delta^3 \kappa^{-3}\rho_\alpha\rho_\beta\rho_\gamma\rho_\delta$$

$$+\tfrac{1}{16}\sum_\alpha \frac{\beta^2\hbar^2 e_\alpha^2}{m_\alpha}\kappa^3\rho_\alpha-\tfrac{3}{4}\sum_{\alpha,\beta}\beta e_\alpha e_\beta \kappa\rho_\alpha\rho_\beta \lim_{R\to\infty}\{\ \}+O(\rho^3\ln\rho) \ , \tag{5.4}$$

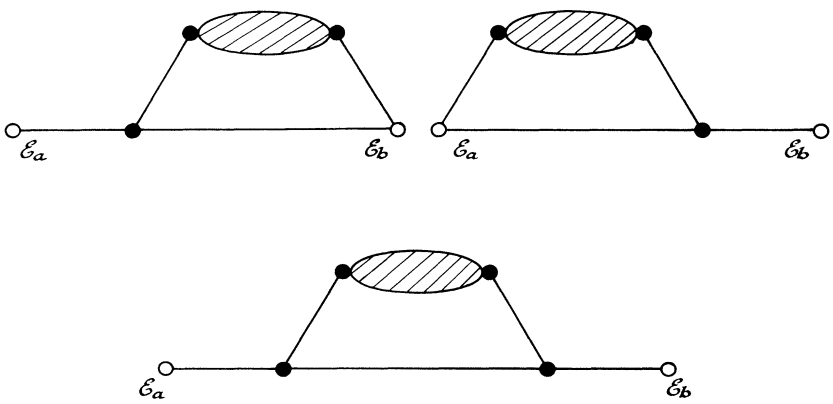

FIG. 13. The three graphs obtained by convoluting the graph shown in Fig. 12 with one or two bonds f_D.

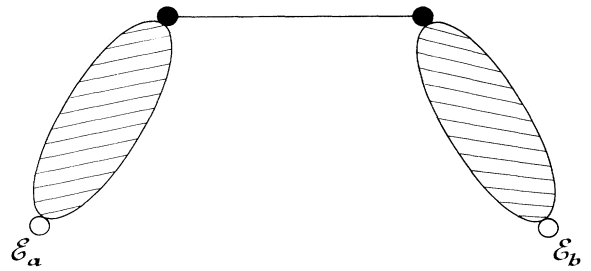

FIG. 14. The chain graph Π_{chain} ($N=2, M_R=2, M_D=1$).

where $\lim_{R\to\infty}\{\ \}$ is the truncated trace of $\exp(-\beta h_{\alpha\beta})$ appearing in (4.21).

The calculations of the quantities that are related to the free energy via partial differentiations with respect to the temperature, like the internal energy or the specific heat at constant volume, for instance, require the knowledge of the temperature dependence of the virial coefficients of the density expansion (4.21). For the classical and diffraction terms, these coefficients merely reduce to polynomials in β. The temperature dependence of the short-range quantum contributions enters in the truncated trace of $\exp(-\beta h_{\alpha\beta})$, for which, to our knowledge, no simple analytic expressions are available in the literature. However, there exist high-temperature expansions, the coefficients of which are all known in terms of Riemann's functions [17]. Eventually, all the other thermodynamic functions (like the adiabatic coefficients, for instance) are calculated in terms of the above virial coefficients by combining thermodynamic identities and relations between Jacobians.

We recall that all the present density expansions have been calculated in the framework of Maxwell-Boltzmann statistics. The exchange contributions will be included in a future paper.

APPENDIX

In this Appendix, we derive a differentiation trace identity for the Coulomb Hamiltonian $h^g_{\alpha\beta}=-\hbar^2/(2m_{\alpha\beta})\Delta+gv_{\alpha\beta}(r)$ with $v_{\alpha\beta}(r)=e_\alpha e_\beta v_c(r)$, which is the extension of the familiar identity

$$\beta\mathrm{Tr}\{V_{\text{int}}\exp[-\beta(h^0_{\alpha\beta}+gV_{\text{int}})]\}$$
$$=-\frac{\partial}{\partial g}\mathrm{Tr}\{\exp[-\beta(h^0_{\alpha\beta}+gV_{\text{int}})]-\exp(-\beta h^0_{\alpha\beta})\}\ , \tag{A1}$$

valid for any integrable potential $V_{\text{int}}(\mathbf{r})$. Of course, in the present case, the traces have to be defined via suitable truncations, which eliminate the long-range Coulomb divergencies and we set

$$I_g=\int d\mathbf{r}\left[(2\pi\lambda^2_{\alpha\beta})^{3/2}\langle\mathbf{r}|\exp(-\beta h^g_{\alpha\beta})|\mathbf{r}\rangle-1+g\beta v_{\alpha\beta}(r)\right.$$
$$\left.-\frac{g^2}{2}\beta^2v^2_{\alpha\beta}(r)+\frac{g^3}{6}\beta^3v^3_{\alpha\beta}(r)g(r)\right]\ , \tag{A2}$$

where $g(r)$ is a given function of r such that $g(r)\sim\text{const}\times r$ when $r\to0$, and $g(r)\to1$ when $r\to\infty$. Using

$$\frac{\partial}{\partial g}\langle\mathbf{r}|\exp(-\beta h^g_{\alpha\beta})|\mathbf{r}\rangle=-\int_0^\beta d\tau\int d\mathbf{r}'\langle\mathbf{r}|\exp[-(\beta-\tau)h^g_{\alpha\beta}]|\mathbf{r}'\rangle v_{\alpha\beta}(r')\langle\mathbf{r}'|\exp(-\tau h^g_{\alpha\beta})|\mathbf{r}\rangle\ , \tag{A3}$$

which follows from the Dyson equation, we find

$$\frac{\partial}{\partial g}I_g=-\int d\mathbf{r}\int d\mathbf{r}'\,\psi_g(\mathbf{r},\mathbf{r}')\ , \tag{A4}$$

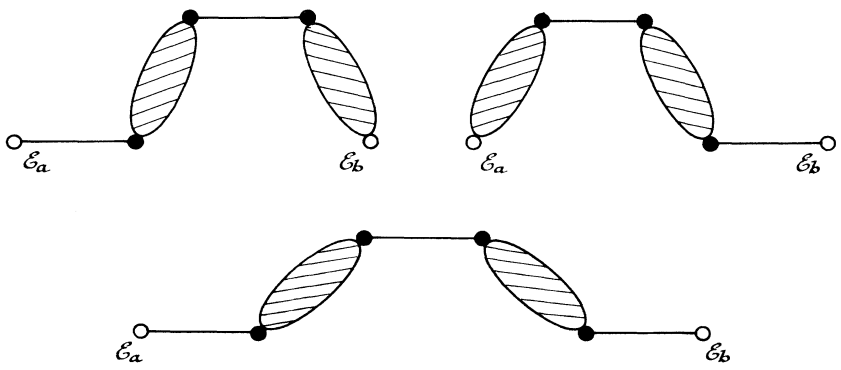

FIG. 15. The three graphs obtained by convoluting the graph shown in Fig. 14 with one or two bonds f_D.

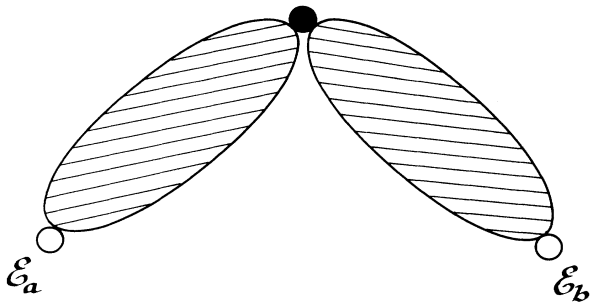

FIG. 16. The chain graph Π_{chain} ($N=1, M_R=2$).

with

$$\psi_g(\mathbf{r},\mathbf{r}')=v_{\alpha\beta}(r')\left\{(2\pi\lambda_{\alpha\beta}^2)^{3/2}\int_0^\beta d\tau\langle\mathbf{r}|\exp[-(\beta-\tau)h_{\alpha\beta}^g]|\mathbf{r}'\rangle\langle\mathbf{r}'|\exp(-\tau h_{\alpha\beta}^g)|\mathbf{r}\rangle\right.$$
$$\left.-\beta\delta(\mathbf{r}-\mathbf{r}')\left[1-g\beta v_{\alpha\beta}(r)+\frac{g^2\beta^2}{2}v_{\alpha\beta}^2(r)g(r)\right]\right\}. \tag{A5}$$

The integral in the right-hand side of (A4) is not absolutely convergent because, when $\mathbf{r}$ and $\mathbf{r}'$ are sent simultaneously to infinity, $\psi_g(\mathbf{r},\mathbf{r}')$ decays as the Coulomb potential itself, which is not integrable. In fact, we can rewrite $\psi_g(\mathbf{r},\mathbf{r}')$ as

$$\psi_g(\mathbf{r},\mathbf{r}')=\psi_g(\mathbf{r}',\mathbf{r})+D_g^{(\text{as})}(\mathbf{r},\mathbf{r}')+R_g(\mathbf{r},\mathbf{r}'), \tag{A6}$$

where $D_g^{(\text{as})}(\mathbf{r},\mathbf{r}')$ is the nonabsolutely integrable asymptotic part of the difference $[\psi_g(\mathbf{r},\mathbf{r}')-\psi_g(\mathbf{r}',\mathbf{r})]$,

$$D_g^{(\text{as})}(\mathbf{r},\mathbf{r}')=[v_{\alpha\beta}(r')-v_{\alpha\beta}(r)]\left[1-g\beta\int_0^1 ds\, v_{\alpha\beta}[(1-s)\mathbf{r}'+s\mathbf{r}]\right]$$
$$\times(2\pi\lambda_{\alpha\beta}^2)^{3/2}\int_0^\beta d\tau\langle\mathbf{r}|\exp[-(\beta-\tau)h_{\alpha\beta}^0]|\mathbf{r}'\rangle\langle\mathbf{r}'|\exp(-\tau h_{\alpha\beta}^0)|\mathbf{r}\rangle, \tag{A7}$$

and $R_g(\mathbf{r},\mathbf{r}')$ is the corresponding rest,

$$R_g(\mathbf{r},\mathbf{r}')=[v_{\alpha\beta}(r')-v_{\alpha\beta}(r)](2\pi\lambda_{\alpha\beta}^2)^{3/2}\int_0^\beta d\tau\left\{\langle\mathbf{r}|\exp[-(\beta-\tau)h_{\alpha\beta}^g]|\mathbf{r}'\rangle\langle\mathbf{r}'|\exp(-\tau h_{\alpha\beta}^g)|\mathbf{r}\rangle\right.$$
$$-\langle\mathbf{r}|\exp[-(\beta-\tau)h_{\alpha\beta}^0]|\mathbf{r}'\rangle\langle\mathbf{r}'|\exp(-\tau h_{\alpha\beta}^0)|\mathbf{r}\rangle$$
$$\left.\times\left[1-g\beta\int_0^1 ds\, v_{\alpha\beta}[(1-s)\mathbf{r}'+s\mathbf{r}]\right]\right\}. \tag{A8}$$

In (A7) and (A8), $h_{\alpha\beta}^0$ is the purely kinetic Hamiltonian, $h_{\alpha\beta}^0=-\hbar^2/(2m_{\alpha\beta})\Delta$. Inserting (A6) in (A4), we obtain

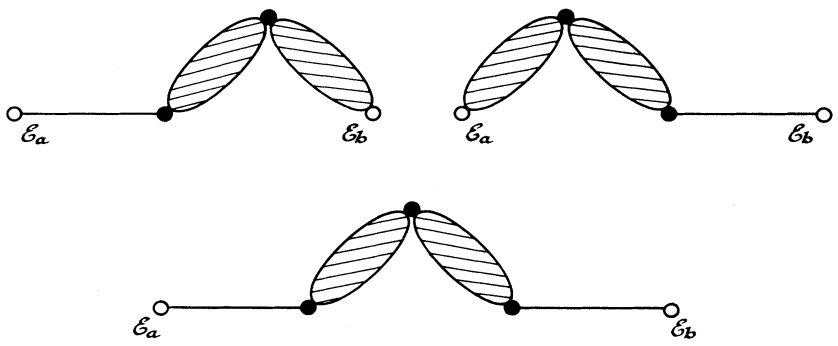

FIG. 17. The three graphs obtained by convoluting the graph shown in Fig. 16 with one or two bonds f_D.

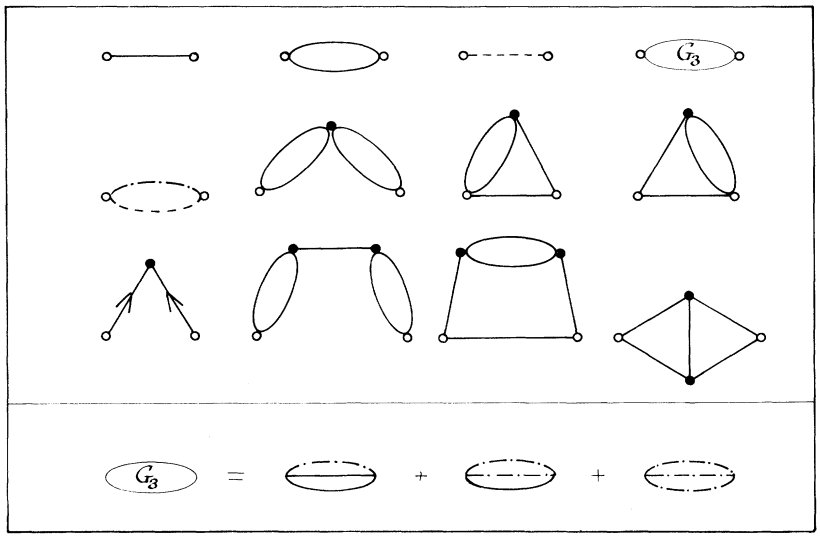

FIG. 18. The 12 primary graphs G_{II}^{scaled}, which contribute to the expansion (4.21) of the free energy (all the other graphs obtained by convoluting these primary graphs with one or two bonds f_D are not drawn). The dashed-dotted lines represent bonds $\kappa H_1(x)$. The bubble with the symbol G_3 inside represents the function $\kappa^3 G_3$, which appears in the scaling decomposition (3.7). At the present order $\rho^{5/2}$, this function can be replaced by $(\kappa^3 f_D^2 H_1/2+\kappa^3 f_D H_1^2/2+\kappa^3 H_1^3/6)$, as illustrated at the bottom of the figure.

$$\frac{\partial}{\partial g} I_g = -\beta \int d\mathbf{r}\, v_{\alpha\beta}(r) \left[(2\pi\lambda_{\alpha\beta}^2)^{3/2} \langle \mathbf{r}|\exp(-\beta h_{\alpha\beta}^g)|\mathbf{r}\rangle - 1 + g\beta v_{\alpha\beta}(r) - \frac{g^2}{2}\beta^2 v_{\alpha\beta}^2(r) g(r) \right]$$
$$- \int d\mathbf{r} \int d\mathbf{r}'\, D_g^{(\text{as})}(\mathbf{r},\mathbf{r}') - \int d\mathbf{r} \int d\mathbf{r}'\, R_g(\mathbf{r},\mathbf{r}') \,, \tag{A9}$$

where we have used the closure relation $\int d\mathbf{r}'|\mathbf{r}'\rangle\langle\mathbf{r}'| = 1$. The nonabsolutely convergent integral with $D_g^{(\text{as})}$ can be evaluated by expanding $[v_{\alpha\beta}(r')-v_{\alpha\beta}(r)]$ and $v_{\alpha\beta}[(1-s)\mathbf{r}'+s\mathbf{r}]$ in Taylor series with respect to $(\mathbf{r}'-\mathbf{r})$ and $(1-s)(\mathbf{r}'-\mathbf{r})$, respectively. Taking into account the harmonicity of the Coulomb potential $[\Delta v_c(r) = -4\pi\delta(\mathbf{r})]$ and the symmetries of the matrix elements of $\exp(-\tau h_{\alpha\beta}^0)$, we find that only one term in these series contributes, i.e.,

$$\int d\mathbf{r} \int d\mathbf{r}'\, D_g^{(\text{as})}(\mathbf{r},\mathbf{r}) = \int d\mathbf{r} \int d\mathbf{r}' \frac{1}{2!} \sum_{\mu\nu} (r'_\mu - r_\mu)(r'_\nu - r_\nu) \frac{\partial^2 v_{\alpha\beta}}{\partial r_\mu \partial r_\nu} \frac{1}{(2\pi\lambda_{\alpha\beta}^2)^{3/2}}$$
$$\times \int_0^\beta d\tau \frac{\beta^3}{\tau^{3/2}(\beta-\tau)^{3/2}} \exp\left[-\left[\frac{\beta}{\tau} + \frac{\beta}{(\beta-\tau)} \right] \frac{(\mathbf{r}-\mathbf{r}')^2}{2\lambda_{\alpha\beta}^2} \right]$$
$$= \tfrac{1}{6} \int d\mathbf{r}\, \Delta v_{\alpha\beta}(r) \frac{1}{(2\pi\lambda_{\alpha\beta}^2)^{3/2}} \int_0^\beta d\tau \frac{\beta^3}{\tau^{3/2}(\beta-\tau)^{3/2}} \int d\mathbf{t}\, t^2 \exp\left[-\frac{\beta^2 t^2}{2\tau(\beta-\tau)\lambda_{\alpha\beta}^2} \right] = -\frac{\pi}{3}\beta e_\alpha e_\beta \lambda_{\alpha\beta}^2 \,. \tag{A10}$$

As it can be seen from the Feynman-Kac representation of the matrix elements of $\exp(-\tau h_{\alpha\beta}^g)$,

$$\langle \mathbf{r}'|\exp(-\tau h_{\alpha\beta}^g)|\mathbf{r}\rangle = \frac{\exp\left[-\frac{\beta(\mathbf{r}-\mathbf{r}')^2}{2\tau\lambda_{\alpha\beta}^2} \right]}{(2\pi\lambda_{\alpha\beta}^2)^{3/2}} \int \mathcal{D}(\xi) \exp\left[-\tau g \int_0^1 ds\, v_{\alpha\beta}[(1-s)\mathbf{r}+s\mathbf{r}'+\lambda_{\alpha\beta}\xi(s)] \right] \,,$$

$R_g(\mathbf{r},\mathbf{r}')$ remains integrable for any spatial configuration. Consequently, the integral with $R_g(\mathbf{r},\mathbf{r}')$ is absolutely convergent, and it vanishes because of the antisymmetry of R_g, i.e., $R_g(\mathbf{r},\mathbf{r}') = -R_g(\mathbf{r}',\mathbf{r})$. Combining this result to (A10) and (A9), we infer the required identity

$$\beta \int d\mathbf{r}\, v_{\alpha\beta}(r) \left[(2\pi\lambda_{\alpha\beta}^2)^{3/2} \langle \mathbf{r}|\exp(-\beta h_{\alpha\beta}^g)|\mathbf{r}\rangle - 1 + g\beta v_{\alpha\beta}(r) - \frac{g^2}{2}\beta^2 v_{\alpha\beta}^2(r) g(r) \right]$$
$$= -\frac{\partial}{\partial g} \int d\mathbf{r} \left[(2\pi\lambda_{\alpha\beta}^2)^{3/2} \langle \mathbf{r}|\exp(-\beta h_{\alpha\beta}^g)|\mathbf{r}\rangle - 1 + g\beta v_{\alpha\beta}(r) - \frac{g^2\beta^2}{2} v_{\alpha\beta}^2(r) + \frac{g^3}{6}\beta^3 v_{\alpha\beta}^3(r) g(r) \right] + \frac{\pi}{3}\beta e_\alpha e_\beta \lambda_{\alpha\beta}^2 \,. \tag{A11}$$

A first difference between the identities (A1) and (A11) is the presence of the substracted terms built with $v_{\alpha\beta}$ and g, which ensure the convergence of the integrals over $\mathbf{r}$ in (A11). The additional term $(\pi/3)\beta e_\alpha e_\beta \lambda_{\alpha\beta}^2$ is more subtle and, to our knowledge, has always been omitted in the literature. It arises from the long-range nature of the Coulomb potential, which prevents the inversion of the integrals over $\mathbf{r}$ and $\mathbf{r}'$ in (A4). It can then be interpreted as resulting from a diffraction effect (as suggested by its structure). We have checked the identity (A11) when the charge e_α and e_β have the same sign, i.e., $e_\alpha e_\beta = e^2$. In this repulsive case, both integrals in (A11) remain finite in the classical limit and can be expanded in powers of $\hbar^2$. The presence of the above diffraction term ensures that the Wigner-Kirkwood expansions of both sides of (A11) are identical, as it should be.

Both convergent integrals in (A11) can be rewritten as finite integrals $\int_{r<R} d\mathbf{r}$ over a sphere of radius R plus terms that go to zero when $R \to \infty$ uniformly with respect to g. The identity (A11) then becomes

$$\beta \int_{r<R} d\mathbf{r}\, v_{\alpha\beta}(r) \left[(2\pi\lambda_{\alpha\beta}^2)^{3/2} \langle \mathbf{r}|\exp(-\beta h_{\alpha\beta}^g)|\mathbf{r}\rangle - 1 + g\beta v_{\alpha\beta}(r) - \frac{g^2}{2}\beta^2 v_{\alpha\beta}^2(r) g(r) \right]$$
$$= -\frac{\partial}{\partial g} \int_{r<R} d\mathbf{r} \left[(2\pi\lambda_{\alpha\beta}^2)^{3/2} \langle \mathbf{r}|\exp(-\beta h_{\alpha\beta}^g)|\mathbf{r}\rangle - 1 + g\beta v_{\alpha\beta}(r) - \frac{g^2}{2}\beta^2 v_{\alpha\beta}^2(r) + \frac{g^3}{6}\beta^3 v_{\alpha\beta}^3(r) g(r) \right] + \frac{\pi}{3}\beta e_\alpha e_\beta \lambda_{\alpha\beta}^2 \tag{A12}$$

disregarding uniformly decaying terms in the limit $R \to \infty$. Each integral $\int_{r<R} d\mathbf{r}$ reduces to a sum of similar integrals associated to the terms appearing in the truncated quantities $[(2\pi\lambda_{\alpha\beta}^2)^{3/2} < \mathbf{r}|\exp(-\beta h_{\alpha\beta}^g)|\mathbf{r}\rangle - \cdots]$ (all these integrals do converge because the integration domain is finite). The corresponding integrals of the substracted terms obviously cancel out side to side, and (A12) becomes

$$\beta \int_{r<R} d\mathbf{r}\, v_{\alpha\beta}(r)(2\pi\lambda_{\alpha\beta}^2)^{3/2} \langle \mathbf{r}|\exp(-\beta h_{\alpha\beta}^g)|\mathbf{r}\rangle = -\frac{\partial}{\partial g} \int_{r<R} d\mathbf{r}(2\pi\lambda_{\alpha\beta}^2)^{3/2} \langle \mathbf{r}|\exp(-\beta h_{\alpha\beta}^g)|\mathbf{r}\rangle + \frac{\pi}{3}\beta e_\alpha e_\beta \lambda_{\alpha\beta}^2 , \tag{A13}$$

disregarding terms which go to zero when $R \to \infty$ uniformly with respect to g. The identity (A13) is, of course, equivalent to (A11). This finite-domain version of the differentiation trace identity is the most convenient for the calculations of the graphs carried out in the main text.

[1] A. Alastuey, F. Cornu, and A. Perez, Phys. Rev. E **49**, 1077 (1994).

[2] J. Ginibre, in *Statistical Mechanics and Quantum Field Theory,* 1971 Les Houches Lectures, edited by C. de Witt and R. Stora (Gordon and Breach, New York, 1971).

[3] See, e.g., B. Simon, *Functional Integration and Quantum Physics* (Academic, New York, 1979).

[4] J. E. Mayer and M. G. Mayer, *Statistical Mechanics* (Wiley, New York, 1940); J. E. Mayer and E. Montroll, J. Chem. Phys. **9**, 2 (1941).

[5] J. E. Mayer, J. Chem. Phys. **18**, 1426 (1950).

[6] E. E. Salpeter, Ann. Phys. (N.Y.) **5**, 183 (1958).

[7] E. Meeron, J. Chem. Phys. **28**, 630 (1958); *Plasma Physics* (McGraw-Hill, New York, 1961).

[8] R. Abe, Progr. Theor. Phys. **22**, 213 (1959).

[9] D. Brydges and P. Federbuch, in *Rigorous Atomic and Molecular Physics,* Vol. 74 of *NATO Advanced Study Institute, Series B: Physics,* edited by G. Velo and A. S. Wightman (Plenum, New York, 1981); D. Brydges and E. Seiler, J. Stat. Phys. **42**, 405 (1986).

[10] A. Alastuey and Ph. A. Martin, Phys. Rev. A **40**, 6485 (1989); F. Cornu and Ph. A. Martin, *ibid.* **44**, 4893 (1991).

[11] H. Friedman, *Ionic Solution Theory* (Interscience, New York, 1962).

[12] E. H. Lieb and J. L. Lebowitz, Adv. Math. **9**, 316 (1972).

[13] A. Alastuey and A. Perez, Europhys. Lett. **20**, 19 (1992).

[14] T. Morita, Prog. Theor. Phys. Jpn. **22**, 757 (1959).

[15] W. Ebeling, Ann. Phys. (Leipzig) **19**, 104 (1967).

[16] W. Ebeling, W. D. Kraeft, and D. Kremp, *Theory of Bound States and Ionization Equilibrium in Plasmas and Solids* (Akademie, Berlin, 1976).

[17] W. D. Kraeft, D. Kremp, W. Ebeling, and G. Röpke, *Quantum Statistics of Charged Particle Systems* (Plenum, New York, 1986).

[18] See, A. Alastuey, in *The Equation of State in Astrophysics,* edited by G. Chabrier and E. Schatzman (Cambridge University Press, Cambridge, 1994). This review paper includes a simple presentation of the effective-potential method and of the many-body perturbation theory.

[19] E. L. Pollock and J. P. Hansen, Phys. Rev. A **8**, 3110 (1973).

[20] E. G. D. Cohen and T. J. Murphy, Phys. Fluids **12**, 1404 (1969).

[21] See, e.g., A. L. Fetter and J. D. Walecka, *Quantum Theory of Many Particle Systems* (McGraw-Hill, New York, 1971).

[22] E. W. Montroll and J. C. Ward, Phys. Fluids **1**, 55 (1958).

[23] A. Sakakura, Ph.D. thesis, University of Colorado, 1960; H. E. DeWitt, J. Nucl. Energy Part C **2**, 27 (1961).

[24] H. E. DeWitt, J. Math. Phys. **3**, 1216 (1962); *ibid.* **7**, 616 (1966).

[25] F. J. Rogers, Phys. Rev. A **10**, 2441 (1974).

[26] For a review, see, e.g., F. J. Rogers, in *The Equation of State in Astrophysics* (Ref. [18]).
[27] M. Lavaud, J. Stat. Phys. **19**, 429 (1978).
[28] These values of C_1 and C_2 are slightly different from those given in Ref. [13]. This difference comes from a better numerical estimation of the dimensionless integrals involved in (4.21).
[29] In fact, part of (4.22) also arises from the diffraction term in the trace identity (A13), which was not properly used in previous calculations.